

The status of neutron-capture elements according to Gaia-ESO

Linnéa Strandell

Lund Observatory
Lund University



2017-EXA125

Degree project of 15 higher education credits
June 2017

Supervisor: Louise Howes

Lund Observatory
Box 43
SE-221 00 Lund
Sweden

Abstract

The aim of this thesis is to get a better understanding of the evolution of the Milky Way stellar disc by looking at the abundance ratios for neutron-capture elements in thin and thick disc stars.

In this project the formation of our Galaxy's thin and thick disc was studied by analysing 10 different neutron-capture elements in field stars measured by Gaia-ESO. The methodology to determine if this new data by Gaia-ESO was reliable was first to match the new data to existing done by Fulbright (2000), Koch & Edvardsson (2002), Yong et al. (2005), Carretta et al. (2011) and Battistini & Bensby (2016). By fitting synthesised spectra to match the observed spectra, the limit for the lowest signal-to-noise ratio for trustworthy measurements was determined and the calculated abundance ratio were compared to the measured ones to verify the new data.

Abundance results for up to 1486 stars are presented for Y, Zr, Mo, Ba, La, Ce, Pr, Nd and Eu. For the abundance ratio, $[x/Fe]$, against the metallicity, $[Fe/H]$, the general trend showed decreasing abundance ratios with increasing metallicity. This suggests that many elements were, relatively to Fe, more abundant in the early Galaxy, when the r -process was more active because of type-II supernovae (SN II) stars. Y and Ba illustrated a more flat tendency which indicates that they are produced via the s -process mostly, from AGB stars that enrich the environment when the Galaxy is older.

The abundance ratio, $[x/Fe]$ as a function of age showed that a change in slope is seen around 8 Gyr for some elements. Thick disc stars show an overall decrease in abundance ratio with respect to younger ages, which is due to the reduction of SN II with time, that causes the slowdown in production of r -process elements. For the thin disc, the general trend is flat, this can be explained by the main enrichment from the AGB stars for the s -process is balanced out by the production of Fe from type-Ia supernovae (SN Ia).

Acknowledgements

Especially, I want to thank my supervisor Louise Howes for her good advice and for helping me complete this thesis. Thanks to Abdalrahman (Abdu) Abohalima for helping me install and learn SME. I also want to thank my family and friends for their support and interest in my work.

Populärvetenskaplig beskrivning

I dagens samhälle kan mycket förklaras med hjälp av fysik, men det finns också väldigt mycket som vi inte kan förklara eller förstår fullt ut. Ett exempel på detta är vår egen galax, Vintergatan. Hur bildades den? Varför ser den ut som den gör? Det finns flera teorier om hur det kan ha gått till, men mycket är ännu oklart för forskare. Teorierna måste testas.

I dag består Vintergatan av många olika delar, bland annat en tunn och en tjock disk. Det går att skilja den tjocka och tunna disken åt genom stjärnornas ålder. De stjärnor som är äldre än 8 miljarder år hittas ofta i den tjocka disken medan stjärnor yngre än 8 miljarder år oftast befinner sig i den tunna disken. Men hur kommer det sig? Genom att undersöka vad stjärnor innehåller för olika ämnen och ser hur det spridit ut sig i galaxen kan man få en bild utav hur Vintergatan har utvecklats.

Det periodiska systemet innehåller många olika ämnen. Många av de tyngre grundämnena, med atomnummer större än 30, som till exempel strontium och yttrium, produceras via neutroninfångning. Neutroninfångning är en process där en neutron krockar med en atomkärna för att tillsammans bilda en tyngre kärna, som när en bil skulle krocka med en annan bil för att bilda en tyngre och större lastbil. Denna process kan ske antingen långsamt eller snabbt, precis som bilar som kan köra i olika hastigheter. De långsamt bildade kärnorna har genomgått en så kallad *s*-process (*s* står för engelskans ”slow”) medan de snabbt bildade har skapats av en *r*-process (*r* står för engelskans ”rapid”). I universum skapas dessa tyngre grundämnen via dessa processer, i antingen explosiva miljöer i *r*-processen fall, medan *s*-processen inträffar i lugnare miljöer.

Det rymdbaserade teleskopet Gaia, och ESO som har markbaserade teleskop, kompletterar varandra genom att mäta olika egenskaper hos stjärnorna i Vintergatan. I detta projekt kommer de neutroninfångade ämnena undersökas då nya mätvärden har tagits fram av Gaia-ESO. I det senaste utsläppet från Gaia-ESO har cirka 54 000 stjärnor mätts på egenskaper så som temperatur, ålder, hur mycket av olika grundämnena de innehåller med mera. Det är många fler stjärnor än vad som använts i tidigare forskning.

Genom att undersöka hur mycket av dessa tyngre neutroninfångade ämnena som finns i stjärnorna i vår galax, går det att se hur ämnena har spridit ut sig. Jämförs de här värden med andra egenskaper hos stjärnan, så som stjärnans ålder och temperatur, kan det gå att få en bättre bild och förståelse kring Vintergatan och hur den har utvecklats. Detta är ett viktigt steg i vår förståelse kring universum och hur galaxer skapas och utvecklas.

Contents

1	Introduction	1
1.1	Neutron-capture elements	1
1.2	Observations of neutron-capture elements in the Milky Way	2
1.3	The Gaia-ESO data	4
1.4	This thesis work	4
2	Method	5
2.1	Confirming the data	5
2.1.1	Match with literature	5
2.1.2	SME	8
3	Results and discussion	11
3.1	Initial results	11
3.1.1	Strontium (Sr)	16
3.1.2	Yttrium (Y)	16
3.1.3	Zirconium (Zr)	17
3.1.4	Molybdenum (Mo)	17
3.1.5	Ruthenium (Ru)	17
3.1.6	Barium (Ba)	17
3.1.7	Lanthanum (La)	18
3.1.8	Cerium (Ce)	18
3.1.9	Praseodymium (Pr)	18
3.1.10	Neodymium (Nd)	19
3.1.11	Samarium (Sm)	19
3.1.12	Europium (Eu)	19
3.2	<i>s</i> - and <i>r</i> -process.	20
3.2.1	[Eu/Ba]	20
3.2.2	Y, Zr	21
3.2.3	La, Ce	22
3.2.4	Mo, Pr	24
3.2.5	Nd, Sm	25

3.3	Abundances ratio compared to age	27
3.4	Position of the stars	30
4	Conclusions	35
4.1	Future work	36
	Appendices	40
A	GES match with literature	i
B	SME example	vi
C	Abundance ratio as a function of temperature	viii

List of Figures

2.1	GES Zr abundance matched with literature abundance.	6
2.2	Abundance difference for [Y/Fe] against S/N and error.	8
3.1	HR-diagram of the selected GES stars.	12
3.1	The [Zr,Ba/Fe] as a function of temperature	13
3.2	The abundance ratio as a function of metallicity.	16
3.3	Abundance combination for [Eu/Ba] against metallicity.	21
3.4	Abundance combination for [Y,Zr/Ba,Eu] against metallicity.	22
3.5	Abundance combination for [La,Ce/Ba,Eu] against metallicity.	23
3.6	Abundance combination for [Mo,Pr/Ba,Eu] against metallicity.	25
3.7	Abundance combination for [Nd,Sm/Ba,Eu] against metallicity.	26
3.8	The abundance ratio as a function of age.	29
3.9	The z-position as a function of age	31
3.10	The absolute z-position against the abundance ratio.	34
A.1	The literature abundance ratio as a function of GES abundance ratio. . . .	ii
A.2	Abundance difference against S/N and error.	v
B.1	Ex. of how SME fitted one of the lines	vii
C.1	The abundance ratio as a function of effective temperature.	x

List of Tables

2.1	Mean absolute deviation.	7
2.2	Standard deviation.	7
2.3	The four different stars chosen to be studied in SME	9
2.4	Analysed elements and spectral lines in SME	9
2.5	Difference between measured and mean abundance for the S/N 212 star. . .	10
2.6	Difference between measured and mean abundance for the S/N 55 star. . .	10
2.7	Difference between measured and mean abundance for the S/N 15 star. . .	10

Chapter 1

Introduction

1.1 Neutron-capture elements

The process that creates new atomic nuclei from existing nucleons is called nucleosynthesis. Elements heavier than iron (Fe) are created through neutron-capture which is one important process of stellar nucleosynthesis. Neutron-capture is a nuclear reaction, where an atomic nucleus merges with neutrons to form a heavier nucleus. This is how heavier elements, with atomic number, $Z > 30$ are formed in stellar interiors (Prialink 2010). Therefore, these elements with $Z > 30$ are called neutron-capture elements (Snedden et al. 2008).

There are two types of reactions that are involved in the process of forming heavier nuclei; neutron-capture and β^- -decay. As more and more neutrons are captured by the nuclei a heavier and heavier isotope is created until it gets unstable. An unstable isotope decays via β^- -decay and creates a new element. If this new element is stable it will continue to capture neutrons. If its unstable it will decay through β^- -decay until a stable nucleus is formed.

A stable nucleus will go through the neutron-capture process exclusively. For an unstable nucleus both processes are plausible. The process of β^- -decay has a constant time-scale, while the time-scale for neutron-capture may change with respect to temperature and density of available neutrons. Depending on these competing reactions the neutron-capture will be either slow or rapid, hence the name s - and r -process. These two processes will differ in outcome and reaction chains (Burbidge et al. (1957) and Prialink (2010)).

The s -process occurs in the Asymptotic Giant Branch (AGB) phase of stellar evolution mostly and in giant stars with a He-burning core and in the convective H-burning shell. The r -process is believed to occur in an explosive environment, although this is uncertain, this is discussed in e.g. Snedden et al. (2008) and Battistini & Bensby (2016) more thoroughly.

The s -process produces almost half the elements from iron (Fe) to bismuth (Bi) and the r -process produces the other half of the elements heavier than Fe. It is very important to understand how, when and where these elements are produced to get a better understanding of our Galaxy (Battistini & Bensby 2016).

The site for the r -process is yet to be discovered and understood. It is proposed that it should take place in an explosive environment, such as a type-II supernova (SN II) or neutron stars mergers (Freiburghaus et al. 1999), but this has not yet been observed, in supernovae or their remnants (Travaglio et al. (2004) and Sneden et al. (2008) for example, discuss this).

The nucleosynthetic model for the lighter s -process peak elements Sr, Y and Zr is not well understood either. Travaglio et al. (2004) studied these elements and by summing up all contributions from their model they saw that 8%, 18% and 18% of Sr, Y and Zr were missing. This missing fraction is assumed to come from "primary" origin from massive stars at low [Fe/H]. Because the process mainly affects the lighter peak elements this additional nucleosynthetic contribution is called lighter element primary process (LEPP) and could explain some differences between these elements.

Due to the work of Arlandini et al. (1999) it is seen that most of the elements are produced through a mixture of s - and r -process. This makes it harder to determine which of the processes are involved when creating the element. There are only a few elements that are produced through one of the two processes (s - and r -process). For example, barium (Ba) is almost only produced through slow neutron-capture, while europium (Eu) is almost created completely through the rapid process. By comparing these two with different elements, it can be seen how abundant they were in the early formation of the Galaxy and more (more recent work on this has been done by Bisterzo et al. (2014) for example).

The r -process is active in the early Galaxy mostly, when more SN II were active. The s -process elements seem to come at least 1 Gyr later, when the AGB stars with a range of $(1 - 8)M_{\odot}$ have developed and begun to enrich their environment. This means that r -process elements should be more present in old stars and s -process elements in younger stars (Battistini & Bensby 2016).

1.2 Observations of neutron-capture elements in the Milky Way

An important work in this field was done by Battistini & Bensby (2016), where they determined and looked at the abundance for seven different neutron-capture elements, for 593 stars in total in our Galaxy. They investigated the elements: Strontium (Sr), Zirconium (Zr), Lanthanum (La), Cerium (Ce), Neodymium (Nd), Samarium (Sm) and Europium (Eu) for these stars. However, it was not possible to measure all the elements in every star.

These abundances were converted into $[x/Fe]$ ratios which were then compared to the overall metallicity, $[Fe/H]$ ¹, one uses Fe as an overall metallicity as its spectra is easy to measure from stars. This was done to see how these abundances were distributed through

¹The overall metallicity is defined as the logarithm of a star's iron abundance ratio compared to the Sun: $[Fe/H] = \log\left(\frac{N_{Fe}}{N_H}\right)_{star} - \log\left(\frac{N_{Fe}}{N_H}\right)_{Sun}$, where N is the number of atoms.

the evolution of the Milky Way and in particular the Solar neighbourhood. Since metallicity can be used as a rough proxy for time, studies have shown that the more metals a star's atmosphere has the younger it should be. For some neutron-capture elements the production site is uncertain and many of them are produced from a mix between the r - and s -process. Therefore, it is good to compare them with Ba and Eu, which are created mostly through the s - and r -process, respectively. They also compared the abundance ratio with stellar ages and saw that they produce different slopes before and after 8 Gyr, which is roughly the age separating thin and thick disc stars.

Battistini & Bensby (2016) found that the abundance ratios for Sr and Zr increased with decreasing metallicity. This indicates that Sr and Zr are more abundant in old stars, although they are mostly produced via the s -process (about 69% and 66% relative to Fe, respectively). This suggests that Fe is produced at a higher rate than Sr and Zr. The La and Ce ratio showed a more flat trend, which is typical for s -process elements like them. The ratio for Nd was tighter than for the other elements and it presented a slight increase for lower metallicities, similar to the Zr ratio. As low metallicity stars often are older, this means that these older stars are more Nd enhanced than young stars. Nd is created through both processes somewhat equally, this indicates that more Fe is being produced in young stars. The abundance ratio for Sm also showed a rising trend from Solar metallicity to lower values. From the [Eu/Fe] ratio they distinguished that it followed an α -element trend, i.e. it was tight and for low metallicity values the [Eu/Fe] ratio was high and decreased as the metallicity increased. This type of tendency is typical for elements that are created almost only through the r -process, as Eu is. Because the r -process was active in the early Galaxy, and Eu is produced almost only through this process, it indicates that Eu is enhanced in old stars that have lower [Fe/H] values. This is the case for Sm as well, as it is produced mainly through the r -process and shows a similar trend to Eu.

From the examination of the abundance ratio as a function of age, Battistini & Bensby (2016) demonstrated that there were different slopes for the thin and thick disc stars for nearly all the elements. For stars older than 8 Gyr, i.e. thick disc stars, the [x/Fe] values compared to age showed that the abundance ratio increased with age for all elements except Ce. Ce displayed a flat trend for thick disc stars instead. For thin disc stars, i.e. stars younger than 8 Gyr, a decrease with age was seen for Sr and Zr. This implies that the thick disc was created by an energetic and fast formation rate that happened before 8 Gyr ago, which means that at a younger age our Galaxy was enriched in certain neutron-capture elements. The r -process could produce large portions of these elements explaining the increase with age for thick disc stars. For La, Ce, Nd, Sm and Eu a flat slope was presented for thin disc stars. This flatness can be due to the contribution from low- and intermediate mass stars in the AGB phase becoming more influential. The Fe production from type-Ia supernovae (SN Ia) is similar to this and this causes the flattening. Neutron-capture elements will also increase at the same rate as the metallicity in young stars in addition to this.

Battistini & Bensby (2016) also compared the [x/H] ratios against the age. The ratio is higher for lower ages, and then it flattens out for ages around 8 Gyr. After 11 Gyr a slight decrease of the abundance was seen. This decrease can be explained by the fact that

these elements were produced via SN II which peaked at roughly 11 Gyr. The increase at younger ages is due to the gas they were formed in being polluted by low-mass stars.

1.3 The Gaia-ESO data

The Gaia-ESO (GES) Public Spectroscopic Survey began taking data on the 31 December 2011, and it will contain spectroscopy for around 10^5 stars in the Milky Way when it is finished (Pancino et al. 2017).

The survey will be a connection between the ground-based telescopes that ESO runs and the space observatory Gaia. For example, Gaia's spectroscopic capabilities are not as good as the large ground-based telescopes, but on the other hand, Gaia will measure the position and parallax, and in that aspect they will complement each other (Gilmore et al. 2012). At Paranal Observatory on the Chilean Andes the multi-object facility FLAMES, which is mounted at the telescope UT2 of the VLT, is used to run this project (Dekker et al. 2000). For this analysis the data from the survey's fourth internal release (iDR4) will be used. It contains observations for around 54 000 stars.

This new data that Gaia-ESO will provide, covers the abundance for some neutron-capture elements in Milky Way stars. Stars that contain neutron-capture elements in this data set are not nearly as many as the total that they have observed, but still a much larger amount than ever looked at before. The Milky Way field stars measured with UVES are the ones focused on in this thesis, which is around 1600 stars. The UVES observations uses a 580 nm set-up. This set-up covers a range of 472-683 nm in wavelength.

1.4 This thesis work

In this paper, the abundances for neutron-capture elements Strontium (Sr), Yttrium (Y), Zirconium (Zr), Molybdenum (Mo), Ruthenium (Ru), Barium (Ba), Lanthanum (La), Cerium (Ce), Praseodymium (Pr), Neodymium (Nd), Samarium (Sm) and Europium (Eu) measured by Gaia-ESO have been studied. Firstly data was checked and confirmed, then by comparing the abundance with the stars' ages, conclusions about the thin and thick disc have been made. The paper is arranged accordingly: Chapter 2 describes the methods for how the abundances were double checked. In Chapter 3 the results of the comparisons are presented and discussed. In Chapter 4 a conclusions and a brief suggestion of future work is made.

Chapter 2

Method

2.1 Confirming the data

The iDR4 data Gaia-ESO provided was double checked and confirmed before producing any results. This was done because no-one has used the neutron-capture data yet, so it needed to be verified. The data were also produced by automatic pipelines, so it is good to make some checks by hand. This was done through some different steps. These steps included matching the data with some stars from the literature, calculating a mean and standard deviation of the difference between GES and the literature, plotting the abundance difference as a function of the abundance error and the signal-to-noise ratio (S/N). The final step was to measure abundance ourselves and to check where the limit for S/N lay, using Spectroscopy Made Easy (SME). The stars with too low S/N, which will be determined in section 2.1.2, must be cut out from the data set because their values will not be trustworthy. All other data processing was done using the software MATLAB R2015a.

2.1.1 Match with literature

The abundances given from GES were absolute, hence, the abundances for the elements studied were converted using:

$$[x/Fe] \equiv A(x)_{star} - A(x)_{Sun} - [Fe/H]_{star} \quad (2.1)$$

Where $A(x)_{star}$ is the abundance measured by Gaia-ESO for a certain element x in a star. The abundance in the Sun, $A(x)_{Sun}$, is then for the same element x . For the Sun's abundances, values derived by Asplund et al. (2009) were used, as most of the different sources we compare with uses literature Solar abundances. The metallicity, $[Fe/H]_{star}$, is the metallicity from the same star measured by GES.

To check if the stars measured by GES differed from already measured stars, all the stars from iDR4 were matched via their right ascension (RA) and declination (Dec) with some stars from the literature, in this case with Fulbright (2000), Koch & Edvardsson (2002),

Yong et al. (2005), Carretta et al. (2011) and Battistini & Bensby (2016). A maximum error of 5 arcsec was used in this match. The abundances from GES were plotted against the abundance given from the literature. An example of the result can be seen in Figure 2.1. The others can be found in Appendix A, Figure A.1.

This was done to examine if they differed significantly from each other. It can be seen from Figure 2.1 and A.1 that they follow a linear relation in most of the cases and that this relation is very close to 1 : 1, which indicates that the measurements from Gaia-ESO are reasonable. It seems like the GES abundances are systematically higher compared to Carretta et al. (2011), which could be because these stars are cluster stars, or that there is some systematic differences. It could also be due to the fact that we use different Solar values, but as Carretta et al. (2011) does not specify where they got their Solar values from, we can not confirm this.

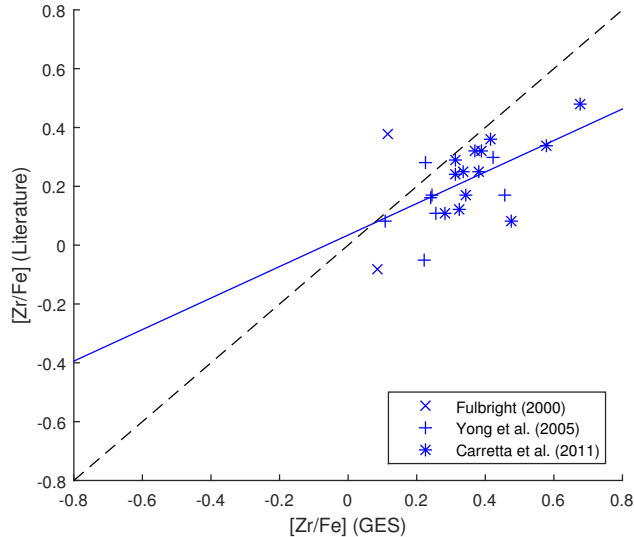


Figure 2.1: The literature $[Zr/Fe]$ vs. the GES $[Zr/Fe]$, together with a linear fit (blue line). The black dashed line is the 1 : 1 ratio.

To see how much the data difference varied the mean and standard deviation were calculated. The mean absolute deviation is defined as follows:

$$\text{mad} = \frac{1}{N} \sum_{i=1}^N |x_i - \bar{x}| \quad (2.2)$$

Where N is the amount of data points, and x is the data point and \bar{x} is the mean value of the data.

The standard deviation was calculated as well for the abundance difference, and it is defined as:

$$\text{sd} = \sqrt{\frac{1}{N-1} \sum_{i=1}^N (x_i - \bar{x})^2} \quad (2.3)$$

The calculated result can be seen in Table 2.1 and 2.2 below.

Table 2.1: Mean absolute deviation of the difference between the GES and literature abundances

[x/Fe]	Fulbright00	Koch02	Yong05	Carretta11	Battistini16
[Sr/Fe]					
[Y/Fe]			0.0421	0.0661	
[Zr/Fe]	0.2137		0.0871	0.0801	
[Ba/Fe]			0.1704	0.1298	
[La/Fe]			0.0130	0.1278	
[Ce/Fe]			0.1087	0.1887	
[Nd/Fe]			0.0416	0.1006	0.0507
[Sm/Fe]					
[Eu/Fe]		0.0540	0.2785	0.0842	0.1061
[Dy/Fe]				0.1298	

Table 2.2: Corrected sample standard deviation of the difference between the GES and literature abundances

[x/Fe]	Fulbright00	Koch02	Yong05	Carretta11	Battistini16
[Sr/Fe]					
[Y/Fe]			0.0521	0.1073	
[Zr/Fe]	0.3023		0.1161	0.1028	
[Ba/Fe]			0.2032	0.1591	
[La/Fe]			0.0184	0.1696	
[Ce/Fe]			0.1590	0.2436	
[Nd/Fe]			0.0525	0.1210	0.0718
[Sm/Fe]					
[Eu/Fe]		0.0701	0.3939	0.1016	0.1402
[Dy/Fe]				0.1591	

This confirmed that the mean and standard deviation for the difference between the GES and literature abundance is low, indicating that the measured abundance by GES is fair. A good match was the [Y/Fe] difference for Yong et al. (2005) with the mean and standard deviation being $\text{mad} = 0.0421$ and $\text{sd} = 0.0521$. The match with Fulbright (2000) for [Zr/Fe] was not as good: $\text{mad} = 0.2137$ and $\text{sd} = 0.3023$, although, these values are not too high, and from Fig. 2.1 we can see this was only based on two data points. The other

literature sources provided better matches for Zr. This confirms that the data from GES, even though some large differences is observed, is in general acceptable enough for the analysis to be useful.

The S/N from (Stonkutė et al. 2016) was plotted with the abundance difference to see if the abundance differences goes up for lower S/N. From Figure 2.2 and A.2 left panel it can be seen that this is not the case. This can be due to Stonkutė et al. (2016) providing good measurements down to S/N around 12 (as we shall see in section 2.1.2), these elements might be easy to measure and are not so affected by the S/N of the rest of the spectrum.

The abundance difference between GES and the literature was plotted as a function of the estimated abundance error measured by GES. This was done to check if the abundance difference increased for higher errors. The right panel of Figure 2.2 and A.2 presents the result of this, and surprisingly the expected result is not seen. One explanation to this can be that the errors GES has provided are not a good representation of the real uncertainty in the measured neutron-capture elements.

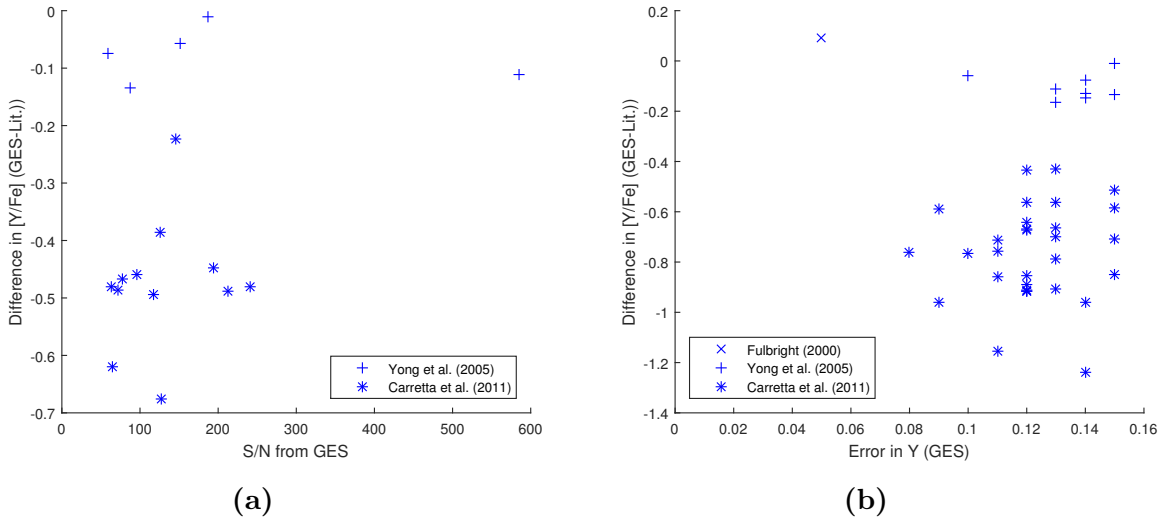


Figure 2.2: *The difference in $[Y/Fe]$ against the signal-to-noise ratio (left panel) or error in Y (right panel).*

2.1.2 SME

The limit where the S/N becomes too low to give accurate measurements was derived using the software program Spectroscopy Made Easy in IDL (SME; Valenti & Piskunov (1996); Valenti & Fischer (2005)). In order to determine a star's stellar parameters, SME produces a synthetic spectrum for a model atmosphere and fits this synthetic spectrum to an observed spectrum. In this case SME was used to identify if the synthetic spectral line fitted the observed spectral line well and to check if the $[x/Fe]$ abundance ratios obtained were accurate, hence, it is a good way to see if GES has measured reasonable abundances values.

Because iDR4 contains measurements for so many stars, all could not be studied in SME. Therefore, four different stars with different S/N were chosen, see Table 2.3. The S/N 212 star had also been matched with Carretta et al. (2011). The spectra contained too many lines to have time to go through them all, thus, only the lines presented in Table 2.4 were reviewed.

Table 2.3: *The four different stars chosen to be investigated in SME are presented here together with their S/N and [Fe/H] values.*

ID (C-name)	S/N	[Fe/H]
05135303-4000431	212.67	-1.072
18260798-2521151	55.17	-0.235
06410841-1629195	15.83	-0.308
23194291-4802030	8.99	-0.151

Table 2.4: *Analysed elements and spectral lines in SME.*

Element	Wavelength, [Å]	EP, [eV]	log gf
La II	5122.990	0.3213	-0.850
La II	6390.480	0.3213	-1.410
Ce II	5187.458	1.2116	0.170
Ce II	5274.229	1.0444	0.130
Ce II	5330.556	0.8694	-0.400
Nd II	5130.590	1.3039	0.450
Nd II	5319.810	0.5502	-0.140
Eu II	6437.631	1.3196	-0.602
Eu II	6437.651	1.3196	-0.640
Eu II	6645.099	1.3797	-0.162
Eu II	6645.114	1.3797	-0.200

Using the MARCS2012 model atmospheres (Gustafsson et al. 2008) which assume LTE and plane-parallel atmospheres in one-dimension, the synthetic spectrum was calculated in SME. The observed spectrum together with the line lists were obtained from GES and Heiter et al. (2015). In SME a resolving power of 47000 was used. The stellar parameters such as the effective temperature, surface gravity and metallicity, were given from iDR4.

For the stars with S/N around 212, 55 and 15, SME fitted the lines well, an example of how SME fitted one of our measured lines for our four different stars can be seen in Appendix B Figure B.1. Tables 2.5 to 2.7 declare that the mean abundance calculated by SME did not differ that much from the measured abundance, for example the difference for the [Eu/Fe] ratio is only 0.052 dex for the S/N 15 star. The only value that stands out is the Ce difference for the matched star, which suggest that the value from Carretta et al. (2011) for this star might be off. The other differences are within the error margin

of 0.5 dex, which accounts for our numerous differences and the fact that only a few lines were measured, and many elements have even better values around 0.2 dex.

For the star with S/N about 9, the synthetic spectrum did not fit the observed spectrum well at all. Hence, it was decided that stars with S/N half-way between 15 and 9, i.e. S/N lower or equal to 12, should be cut out because they probably will not have credible measured values. This bad fit is due to the fact that the lines are too weak compared to the noise, and makes them impossible to measure. Even if the S/N is high for the spectrum, some spectral lines might still be too weak for some elements, which might be a problem later as all lines cannot be checked. Another problem is some strong spectral lines suffer much more from hyperfine splitting (hfs). For example the 5122.990 Å La line experienced this, and although SME models this the fit was still bad for this line which could be due to incorrect atomic data for example, it was later taken out as comparison line in SME due to this problem.

Table 2.5: *The GES/Carretta measured abundance for a star in NGC1851 (S/N \approx 212), the mean abundance from SME and the calculated difference.*

[x/Fe]	GES value/Carretta value	Mean SME value	Difference
[La/Fe]	0.012/0.24	0.280	0.268/0.040
[Ce/Fe]	0.032/0.70	-0.117	-0.149/-0.817
[Nd/Fe]	0.372/0.69	0.725	0.353/0.035
[Eu/Fe]	0.272/0.81	0.630	0.358/-0.180

Table 2.6: *The GES measured abundance for the S/N \approx 55 star, the mean abundance from SME and the calculated difference.*

[x/Fe]	GES value	Mean SME value	Difference
[La/Fe]	-0.005	0.100	0.105
[Ce/Fe]	0.135	-0.137	-0.272
[Nd/Fe]	0.165	0.025	-0.140
[Eu/Fe]	0.285	0.540	0.255

Table 2.7: *The GES measured abundance for the S/N \approx 15 star, the mean abundance from SME and the calculated difference.*

[x/Fe]	GES value	Mean SME value	Difference
[La/Fe]	0.118	0.340	0.222
[Ce/Fe]	0.068	0	-0.068
[Nd/Fe]	0.138	0.025	-0.113
[Eu/Fe]	0.128	0.180	0.052

Chapter 3

Results and discussion

3.1 Initial results

When the data were confirmed and the limit for the S/N decided, we started to analyse the results. iDR4 from GES was now limited according to the criteria stated in the introduction, that is, by the Milky Way field stars measured by UVES and with measurements for our elements. To illustrate our sample, we made a HR-diagram together with the stars' metallicities with the remaining 1486 stars from iDR4. Figure 3.1 presents this, and the metallicity is represented by colour. Using a limit for dwarf stars and giants stars that is around $\log g \approx 3.5$ most of the stars, about 97%, are in the main sequence, so there are not really enough giants to compare trends between giants and dwarfs. We will focus on the dwarf stars. It can, however, be good to see which stars are giants or dwarfs, so henceforth, red dots will represent giant stars with surface gravity $\log g < 3.5$, and blue dots dwarf stars with surface gravity $\log g \geq 3.5$ in all following figures, if not stated otherwise.

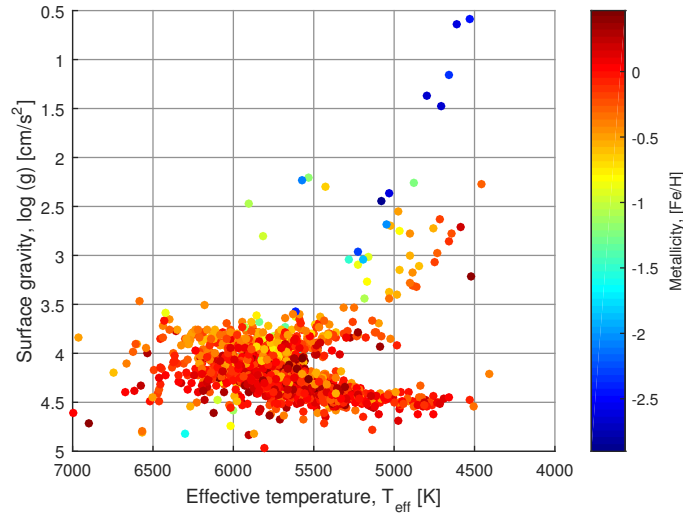


Figure 3.1: *HR-diagram for the UVES stars from iDR_4 with $S/N \geq 12$, plotted as surface gravity against effective temperature. The colour shows the metallicity of the stars.*

The investigated elements abundance ratio, $[x/\text{Fe}]$, were plotted as a function of effective temperature to make sure that no trend was followed. If the abundance ratio has a temperature trend it suggests that something in the measurements are dependent on temperature. Figures 3.1 and C.1 illustrates this for the elements studied. No tendency could be found for any of them except for Ba, see Figure 3.1b. The abundance ratio in this figure shows a slight inclination with increasing temperature. This indicates that something in the measurement of this element is dependent on the temperature. This could be due to the fact that Ba suffers from NLTE at $T_{\text{eff}} > 6100$ K as Korotin et al. (2011) mentions. Due to the fact that no other element followed this trend, this is not discussed any further, but it can be good to bear in mind when discussing Ba.

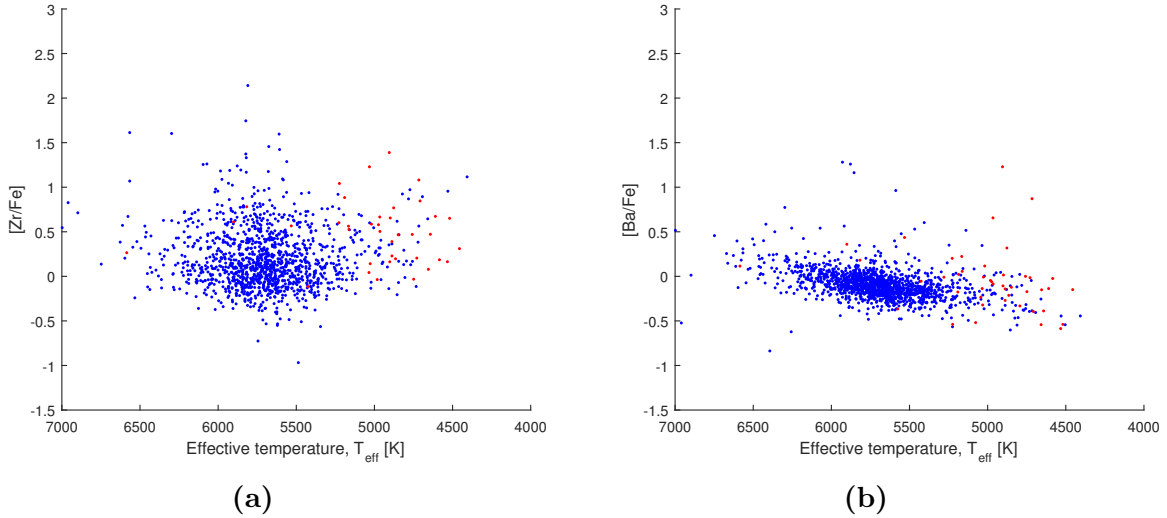
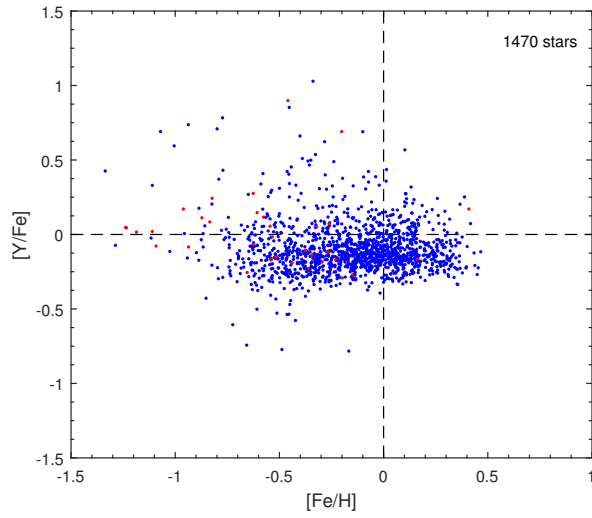


Figure 3.1: The (a) $[Zr/Fe]$ and (b) $[Ba/Fe]$ as a function of temperature

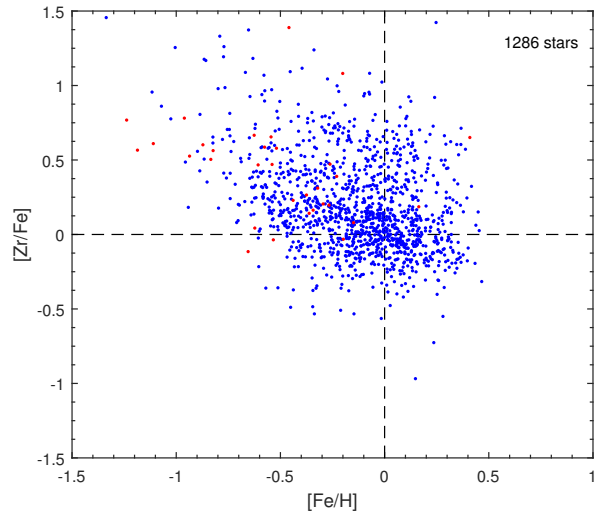
Figure 3.2 shows the abundance ratio as a function of the metallicity, $[Fe/H]$. A few stars showed very low metallicity values, these were cut out from the plot as the results from them might not be as accurate, since we did not double check stars with low metallicity. They are also more likely to be halo stars and not thin or thick disc stars, which are the stars focused on here. A scarce amount of stars also showed high $[x/Fe]$ values, these stars are not seen in the plots either, because they will more likely suffer from some kind of measurement error or unusual abundances caused by stellar evolution which does not tell us anything about the Galaxy. In the future these stars should preferably be investigated even further, to see why they show these high abundance ratios. An error was calculated for all abundance ratios studied, using:

$$[x/Fe]_e = \sqrt{x_e^2 + [Fe/H]_e^2} \quad (3.1)$$

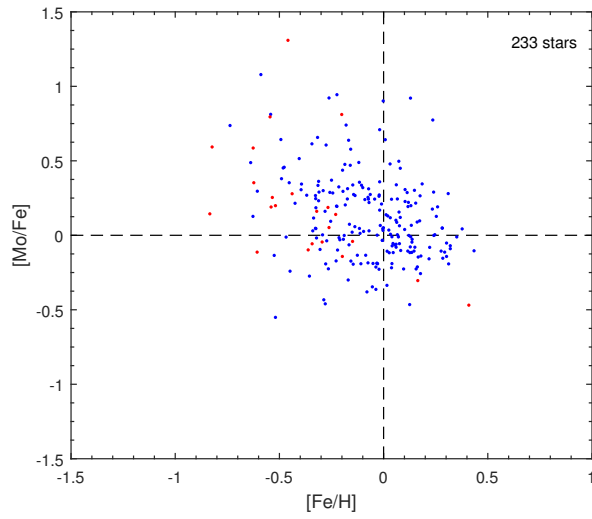
Here, the e stands for error and x is for a certain element. Both the error in a certain element x and $[Fe/H]$ are the measured values from GES. The average error for all abundance ratios was then taken out using this equation.



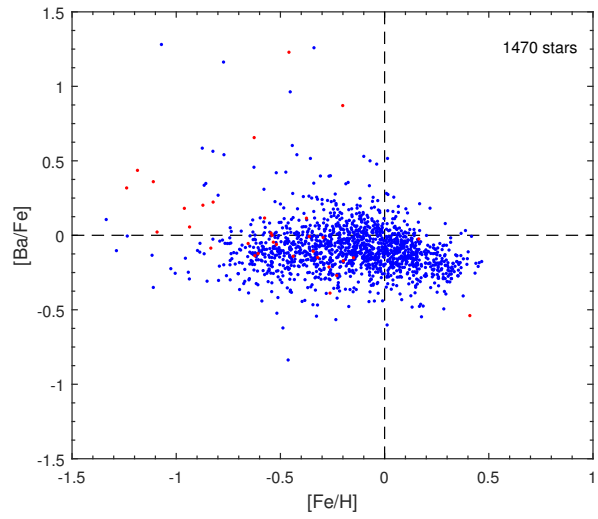
(a)



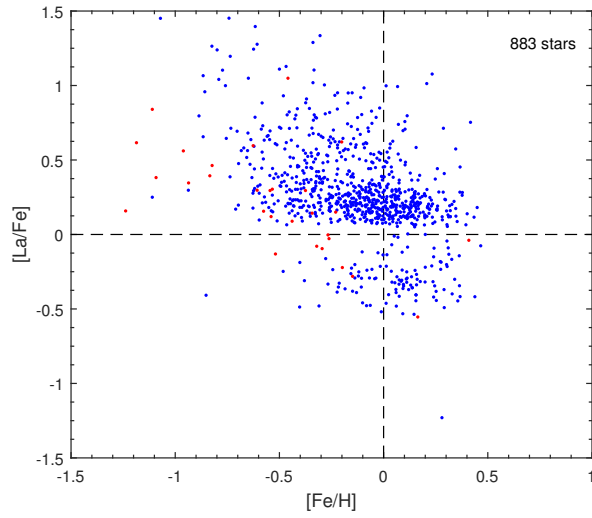
(b)



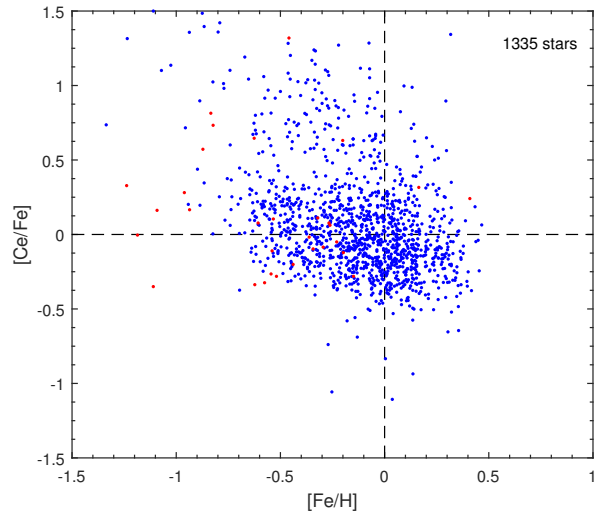
(c)



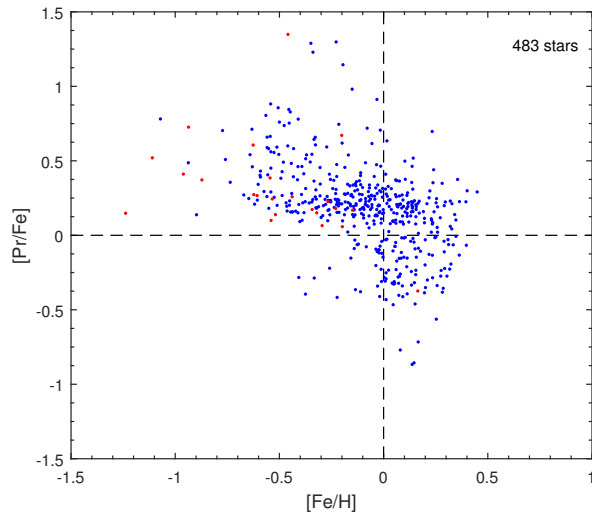
(d)



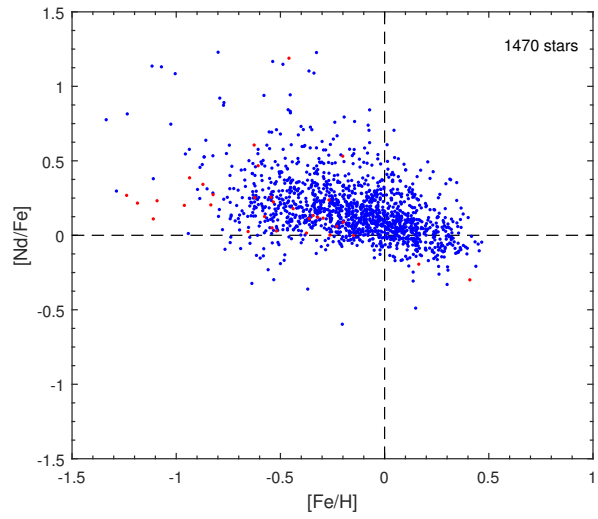
(e)



(f)



(g)



(h)

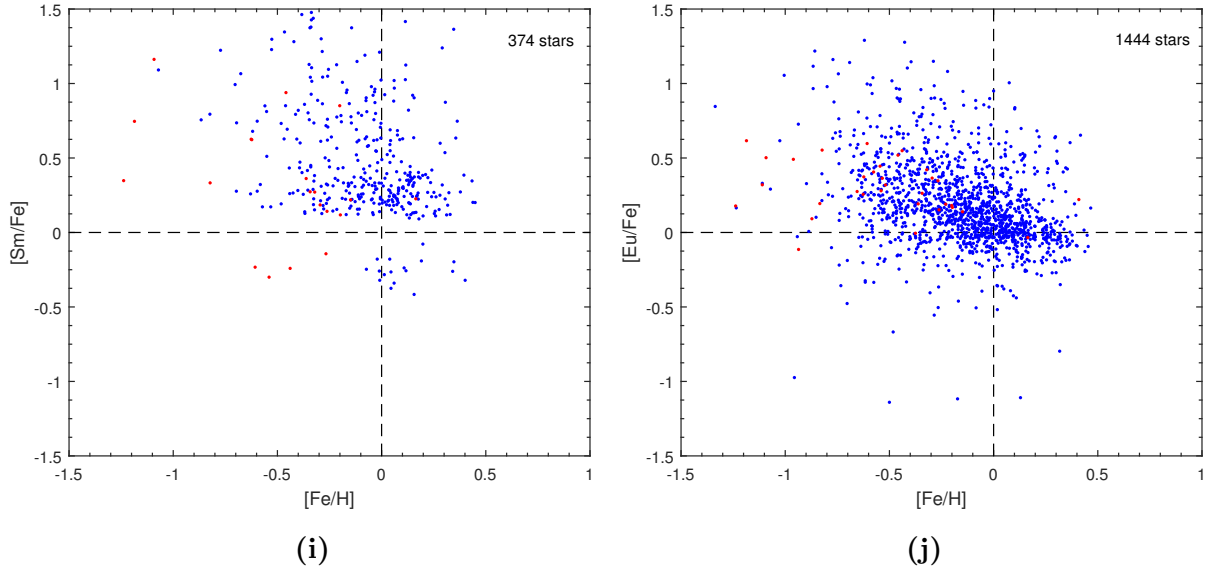


Figure 3.2: The abundance ratio, $[x/Fe]$, as a function of metallicity, $[Fe/H]$. Red dots represent giants and blue dots represent dwarf stars, according to the criteria mentioned earlier.

3.1.1 Strontium (Sr)

Strontium was studied, but due to its very high abundance ratios compared to the literature and after checking the GES line list, it was concluded that the lines were too weak to be measured correctly by GES. Therefore, this element will not be investigated and discussed any further. If this had been checked in SME we might have seen this earlier.

3.1.2 Yttrium (Y)

The abundance ratio, $[Y/Fe]$, plotted as a function of metallicity, $[Fe/H]$, can be seen in Fig. 3.2a. It has in total 1470 stars that are quite spread out at lower metallicity and higher Y ratio. It is fairly flat around $[Y/Fe] \approx -0.1$, and the majority of stars lie around this value. The median error (due to a few really scattered stars) was calculated to be $[Y/Fe]_e = 0.1726$. Mashonkina et al. (2007) showed a basically flat trend around $-1.5 \lesssim [Fe/H] \lesssim 0.1$ for thin and thick disc stars with $[Y/Fe] \approx 0$. The result from Mishenina et al. (2013) also demonstrates this flatness for Y at $-1 \lesssim [Fe/H] \lesssim 0.4$ for $[Y/Fe] \approx 0$. Bensby et al. (2014) studied this element too, they also showed a flat trend. The bulk of the stars had $[Y/Fe]$ values lower than zero just like our result. This flatness in Y suggest that this element has been produced quite evenly in comparison with Fe, since Y suggest that this element has been produced quite evenly in comparison with Fe, since the *s*-process and the higher production rate of Fe (due to SN Ia) kicked in.

3.1.3 Zirconium (Zr)

Figure 3.2b shows a slightly upwards, although more scattered trend compared to Y. The average error was $[\text{Zr}/\text{Fe}]_e = 0.1940$. For lower metallicity the abundance ratio increases from $[\text{Zr}/\text{Fe}] \approx -0.2$ where $[\text{Fe}/\text{H}] \approx 0.3$ to $[\text{Zr}/\text{Fe}] \approx 0.5$ at $[\text{Fe}/\text{H}] \approx -0.6$. The plot contains 1286 stars and for Solar metallicity most of the stars are located at $[\text{Zr}/\text{Fe}] \approx 0$. The same trend was illustrated by Mashonkina et al. (2007), but not as scattered as ours. Mishenina et al. (2013), showed a narrow increase in Zr as the metallicity decreased. Battistini & Bensby (2016) also presents this upwards trend but for a lower number of stars and the trend starts to increase from $[\text{Zr}/\text{Fe}] \approx -0.1$ to 0.3 at $[\text{Fe}/\text{H}] \approx 0.3$ to -1 , respectively. A more flat trend was demonstrated by Burris et al. (2000) and Reddy et al. (2006). Zr is produced by the *s*-process mostly, so a flat trend in abundance should be seen as the AGB stars starts to contribute, just like for Y. This decreasing trend suggest that Zr is more present in old stars, which were enriched by SN II through the *r*-process. This is surprising, but could be due some weak *s*-process formation like, different lighter primary process (LEPP) contributions (Travaglio et al. 2004) or maybe spinstars (Cescutti et al. 2013).

3.1.4 Molybdenum (Mo)

The number of stars is only 233 in Figure 3.2c and they are very spread out. There is a very weak tendency, that for decreasing metallicity the abundance increases. Most of the stars are within the $-0.2 < [\text{Mo}/\text{Fe}] < 0.4$ interval at $-0.4 < [\text{Fe}/\text{H}] < 0.4$, approximately. It is hard to find previous work that look into this neutron-capture element, as it is not well studied. Mo is created by the *r*-process to about 61% so it should show similarities to Sm (which is created by the *r*-process for about 69%) therefore, an increasing trend for lower metallicity is expected. An average error of $[\text{Mo}/\text{Fe}]_e = 0.3050$ was determined, which is quite high.

3.1.5 Ruthenium (Ru)

Because the selected sample from iDR4 only contained measurements for about 44 stars for Ru, this element will not be examined any further. The amount of stars is too low to make any meaningful conclusions about it.

3.1.6 Barium (Ba)

Figure 3.2d shows that the majority of the stars have abundances between $-0.3 < [\text{Ba}/\text{Fe}] < 0.1$ at about $-0.5 < [\text{Fe}/\text{H}] < 0.3$. The figure presents a mostly flat trend for the 1470 stars, with similarities to Y, and with an average error of $[\text{Ba}/\text{Fe}]_e = 0.1734$ also similar to Y. At $[\text{Fe}/\text{H}] = 0$ a downturn in Ba can be seen. Burris et al. (2000) displayed a similar trend for their data set of stars, although, it stretches from $-1 \lesssim [\text{Fe}/\text{H}] \lesssim 1$ for $[\text{Ba}/\text{Fe}]$ around -0.4 to 0.5. A even more flat trend is seen in the studies by Mashonkina et al. (2007)

and Mishenina et al. (2013). Bensby et al. (2014) showed a flat trend for $[\text{Ba}/\text{Fe}] \approx -0.1$ at metallicity around -0.8 to 0. At $[\text{Fe}/\text{H}] \approx 0$ a slight decrease with metallicity is seen, just like for our data. Knowing that Ba, just like Y, is a typical *s*-process element this flatness can be due to that the AGB enrichment by the *s*-process is balanced out by the Fe production rate from SN Ia. Because Ba is a heavy *s*-process element, with supersolar $[\text{Fe}/\text{H}]$, AGB stars produces less, which could explain the downturn.

3.1.7 Lanthanum (La)

Figure 3.2e has a total of 883 stars and the figure shows the $[\text{La}/\text{Fe}]$ ratio as a function of metallicity. A strange gap around $[\text{La}/\text{Fe}] \approx 0$ is seen in the image, and we are yet to figure out why iDR4 does not have any measured data around these values. Otherwise, for decreasing $[\text{La}/\text{Fe}]$ the metallicity increases like for Zr, and the stars are slightly more scattered. Burris et al. (2000) illustrates a more flat trend for the thin and thick disc stars and as the metallicity decreases the stars get more scattered. Mishenina et al. (2013) show a similar trend to ours. This tendency for $[\text{La}/\text{Fe}]$ is also seen in the result by Battistini & Bensby (2016), although, it does not grow as fast and is more tight. The majority of their stars are below $[\text{La}/\text{Fe}] = 0$ and our result shows that the majority of stars lies above. The average error was calculated to be $[\text{La}/\text{Fe}]_e = 0.3492$. The gap causes trouble as it makes it harder to determine if the abundance ratio grows with $[\text{Fe}/\text{H}]$ at all. La is produced mostly through the *s*-process (76% roughly) and as the production rate for Fe increases with time so does La. This suggest that Fe is produced in a higher rate than La, as Fishlock et al. (2014) and Karakas & Lugaro (2016) mentions.

3.1.8 Cerium (Ce)

For $[\text{Ce}/\text{Fe}]$ a total of 1335 stars were included in Figure 3.2f. This picture shows a scattered abundance ratio, this could be due to poor measurement results. Some minor tendency is seen that for subsolar metallicity the Ce ratio increases slightly, like for Zr and La. Most of the stars lie below $[\text{Ce}/\text{Fe}] = 0$ within $-0.6 < [\text{Fe}/\text{H}] < 0.4$. For this element the average error was $[\text{Ce}/\text{Fe}]_e = 0.2493$. The slowly decreasing Ce trend for increasing $[\text{Fe}/\text{H}]$ is presented in Mashonkina et al. (2007) as well, but the majority of stars lie above $[\text{Ce}/\text{Fe}] = 0$. Battistini & Bensby (2016) presents a more flat trend for $[\text{Ce}/\text{Fe}]$, which is in agreement with Mishenina et al. (2013). Although, some of the stars above $[\text{Ce}/\text{Fe}] \approx 0.5$ are quite spread out in our case. Ce is like La, mainly a *s*-process element, so they should show similarities.

3.1.9 Praseodymium (Pr)

The $[\text{Pr}/\text{Fe}]$ abundance ratio has 483 stars and a large average error of $[\text{Pr}/\text{Fe}]_e = 0.3653$. A little gap is seen in Figure 3.2g at $[\text{Pr}/\text{Fe}] \approx 0$. Otherwise, it seems to follow the increasing abundance ratio trend for decreasing metallicity like Zr, La and Ce. Arlandini et al. (1999) investigated this element and showed a quite flat trend at $[\text{Pr}/\text{Fe}] \approx 0.2$. In their case,

only about 20 stars were studied, which might explain our different results. Because Pr is produced by the s - and r -process almost equally it should show some similarities to Nd, and it should show signs of formation at all times.

3.1.10 Neodymium (Nd)

Figure 3.2h of 1470 stars, presents quite a narrow increase in the abundance compared to the other elements and it shows some similarity with Zr, La, Ce and Pr. The narrow increase implies accurate measurements, but it could also be because this element behaves differently. Between $-0.4 < [\text{Fe}/\text{H}] < 0.4$ Nd decreases from $[\text{Nd}/\text{Fe}] \approx 0.4$ to -0.1 . The average error was determined to be $[\text{Nd}/\text{Fe}]_e = 0.2118$. Mishenina et al. (2013) also have this result for Nd although it starts to increase at $[\text{Fe}/\text{H}] \approx 0.2$ to $[\text{Fe}/\text{H}] \approx -0.3$ for $[\text{Nd}/\text{Fe}] \approx -0.2$ to 0.2 , respectively. The trend found by Battistini & Bensby (2016) for this element is quite similar to this, but slightly shifted as it ends at $[\text{Fe}/\text{H}] \approx -0.6$ for $[\text{Nd}/\text{Fe}] \approx 0.2$. Burris et al. (2000), on the other hand, displayed a spread out, flat result. Nd is produced to an extent of 58% by s -process and 42% by the r -process. Depending on the AGB and SN Ia stars ratio, Nd should probably follow a trend similar to the α -elements.

3.1.11 Samarium (Sm)

$[\text{Sm}/\text{Fe}]$ as a function of metallicity is plotted in Figure 3.2i. An amount of 374 stars have been measured. A big void between $-0.2 \lesssim [\text{Sm}/\text{Fe}] \lesssim 0.1$ is seen for this abundance which is yet to be explained, as it should not be there, just like for $[\text{La}/\text{Fe}]$. No obvious trend is seen, most of the stars are scattered and lie in the interval around $-0.4 < [\text{Fe}/\text{H}] < 0.3$. This result is quite different from Mishenina et al. (2013) and Battistini & Bensby (2016), as they discovered a rising trend as the metallicity decreased. Sm is generated by r -process in most cases, and therefore old metal-poor stars should be more Sm enhanced. Decreasing abundance with metallicity is expected. This difference can be due to the gap which makes it hard to determine if a trend is followed or not for Sm. The average error of $[\text{Sm}/\text{Fe}]_e = 0.4320$ is quite high, so these measurements seem less trustworthy.

3.1.12 Europium (Eu)

Eu increases as the metallicity decreases in Figure 3.2j with a total of 1444 stars. The average error was calculated to be $[\text{Eu}/\text{Fe}]_e = 0.2016$. In the region $-0.6 \lesssim [\text{Fe}/\text{H}] \lesssim 0.3$ the abundance increases from $[\text{Eu}/\text{Fe}] \approx -0.1$ to 0.4 respectively. It has some resemblance to Zr, La, Ce and Nd. This increasing trend is presented in Burris et al. (2000), Koch & Edvardsson (2002) and Mishenina et al. (2013) as well. Almost the same α -element trend is observed in Battistini & Bensby (2016), where the Eu abundance ratio increases between $-0.2 < [\text{Eu}/\text{Fe}] < 0.5$ at metallicity around 0.2 to -1 , respectively. As Eu is a typical r -process element it should be enhanced in older stars with low $[\text{Fe}/\text{H}]$ values, as showed in the figure.

3.2 *s-* and *r*-process.

Because barium is almost only made through the *s*-process (around 85%) and europium is created essentially only through the *r*-process (about 94%) (Bisterzo et al. 2014), they are excellent for comparison to other neutron-capture elements, where the production sites are not certain. Therefore, just like Battistini & Bensby (2016), the elements' $[x/\text{Ba}]$ and $[x/\text{Eu}]$ ratios were determined and plotted as a function of metallicity. The product of this is illustrated in Figure 3.3 and Figures 3.4 to 3.7 together with a dotted line which shows where the pure *r*-process lies. This pure *r*-process line was derived from Bisterzo et al. (2014) by subtracting the predicted *s*-process abundance from the Solar System total values.

3.2.1 $[\text{Eu}/\text{Ba}]$

Some of the stars in the $[\text{Eu}/\text{Ba}]$ ratio in Figure 3.3 lie close to the pure *r*-process line. Ba was created via the *r*-process in the young Milky Way, when this was the only process that produced neutron-capture elements in the beginning of the construction of the Galaxy. The abundance ratio for $[\text{Eu}/\text{Ba}]$ decreases with increasing metallicity as expected. This could be due to the AGB stars have had time to start the enrichment of the environment with *s*-process elements. This sort of trend is seen in Battistini & Bensby (2016) as well, although, it is much tighter and out to $[\text{Fe}/\text{H}] \approx -0.8$ at $[\text{Eu}/\text{Ba}] \approx 0.6$, ours is flat and scattered in comparison. These stars are expected to be old therefore. There are a number of stars in the $1 < [\text{Eu}/\text{Ba}] < 1.5$ region, which indicates that the *r*-process yield has been underestimated as these stars are enhanced above the expected values.

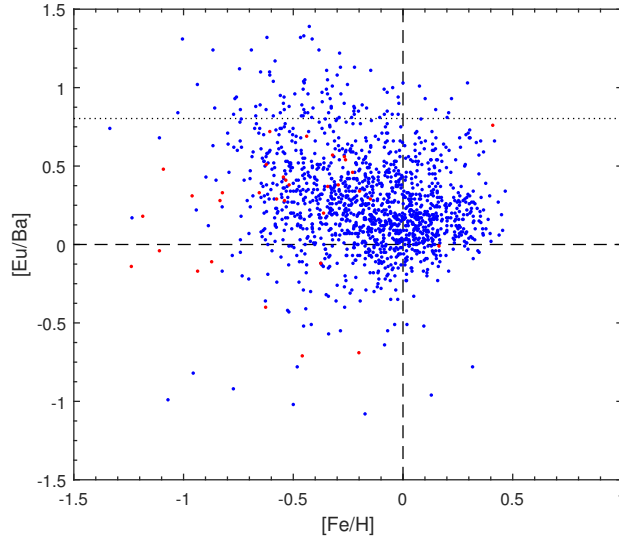


Figure 3.3: *The combined abundance ratio, $[Eu/Ba]$, against the metallicity, $[Fe/H]$. The dotted line represents the pure r -process ratio. Like before, red dots are giants and blue dots are dwarfs.*

3.2.2 Y, Zr

The $[Y,Zr/Ba]$ ratio in Figure 3.4a and b, respectively, are quite different from each other, Y is tight with a flat trend for subsolar metallicities. For $[Fe/H] \approx 0$ it increases in $[Y/Ba]$. Because both Y, Zr are light, and created by the s -process for around 72% and 66%, they should be similar. Zr, on the other hand, is scattered and flat around the $-0.5 < [Fe/H] < 0.5$ region. This scenario is not observed by Battistini & Bensby (2016), as they presented a decreasing $[Zr/Ba]$ trend for increasing metallicity. Many stars lies near the pure r -process ratio for both elements but especially so for Zr.

For the Eu comparison, the $[Y/Eu]$ ratio seems similar to $[Y/Ba]$, but with a tighter trend increasing with increasing metallicity. As the production rate for Eu goes down the rate for Y goes up, meaning that the $[Y/Eu]$ ratio should increase as the stars get younger and the metallicity increases. $[Zr/Eu]$ is like $[Zr/Ba]$, scattered and without any tendency more then a flat one. As Zr is mainly a s -process element the same trend as Y would have been expected. Battistini & Bensby (2016) shows this expected, but not that strong, trend for $[Zr/Eu]$. The difference between Y and Zr could be explained by different lighter element primary process (LEPP) contributions.

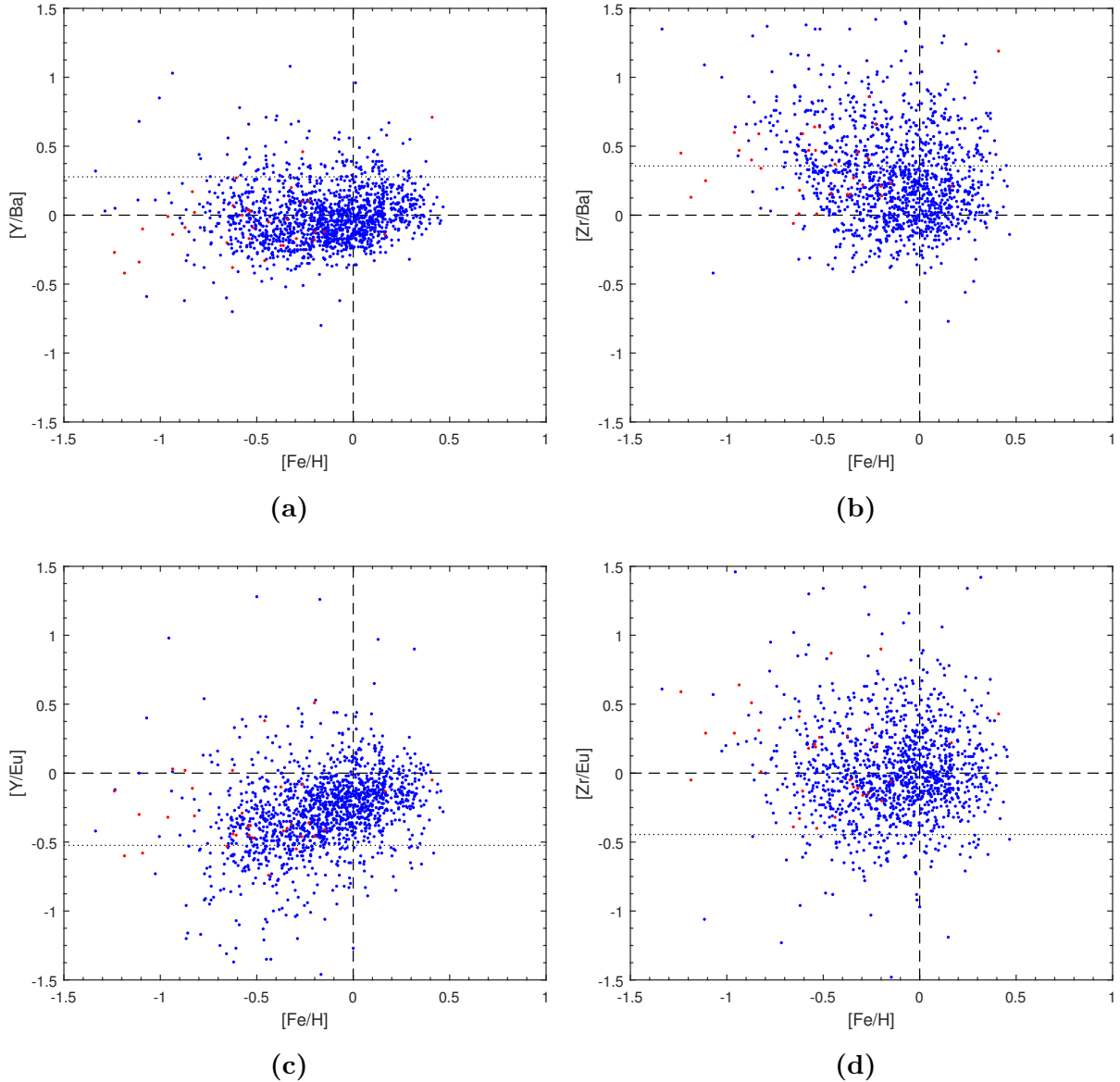


Figure 3.4: $[Y/Ba]$ and $[Zr/Ba]$ (left and right upper panel, respectively) and $[Y/Eu]$ and $[Zr/Eu]$ (left and right bottom panel, respectively) as a function of the metallicity $[Fe/H]$. The dotted line represents the pure r-process ratio.

3.2.3 La, Ce

Figure 3.5 shows the $[La,Ce/Ba,Eu]$ abundance as a function of $[Fe/H]$. The top left panel shows that the $[La/Ba]$ ratio slightly decreases for subsolar metallicity, just like for the $[Eu/Ba]$ case. Because Ba is produced via the s-process at a higher percentage than La the $[La/Ba]$ ratio should decrease as the stars gets more metal-rich. No particular tendency is seen in the Fig. 3.5b and c. Battistini & Bensby (2016) got a different result. A flat trend

was seen for $[La/Ba]$ and $[Ce/Ba]$ but for $[La/Eu]$ and $[Ce/Eu]$ an increase was presented as the metallicity increased, and this increase occurs when the AGB stars starts to enrich their environment by the s -process. As the Eu goes down in production rate both La and Ce should go up as they both are mainly produced through the s -process, meaning that $[La,Ce/Eu]$ ratio should increase with the metallicity. The fact that this is not observed here indicates that we have a large observation scatter and that perhaps we should look at the ages to get a picture of the time-line.

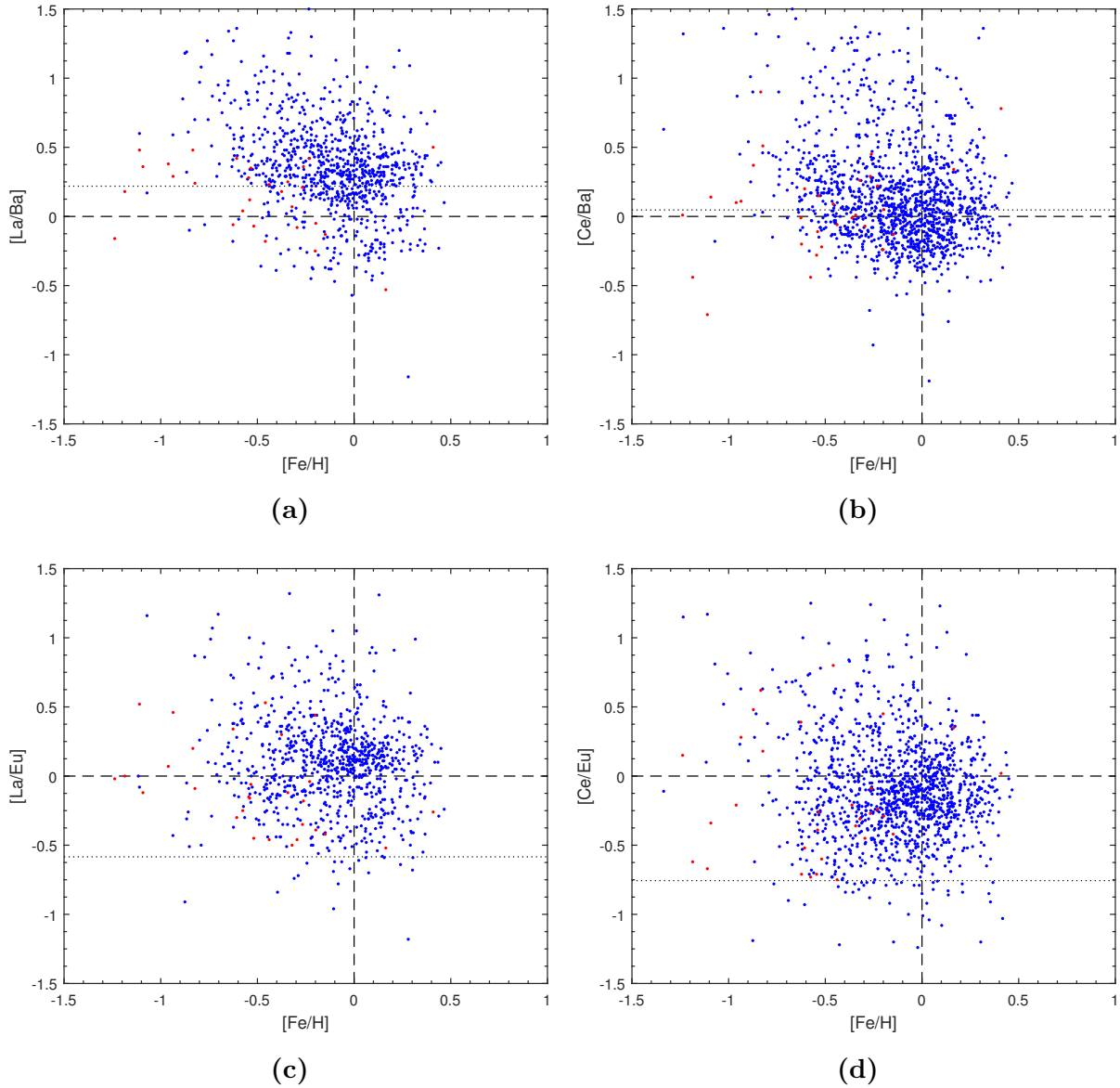


Figure 3.5: $[La/Ba]$ and $[Ce/Ba]$ (left and right upper panel, respectively) and $[La/Eu]$ and $[Ce/Eu]$ (left and right bottom panel, respectively) as a function of the metallicity $[Fe/H]$. The dotted line represents the pure r -process ratio.

3.2.4 Mo, Pr

From Figure 3.6 no trend is noticeable for Fig. 3.6a and c of the abundance ratios. The $[\text{Mo}/\text{Ba}]$ ratio should decrease with $[\text{Fe}/\text{H}]$, as the Ba production rate will go up as soon as the AGB stars start to help with the enrichment and at the same time the Mo rate should go down as the r -process will be less and less active. We cannot see this trend at all for $[\text{Mo}/\text{Ba}]$, probably due to that we have too few stars. A faint trend can maybe be seen in Fig. 3.6a that the abundance increases for lower metallicity. In Fig. 3.6c a vague trend might be seen that for decreasing $[\text{Fe}/\text{H}]$ the $[\text{Mo}/\text{Eu}]$ decrease, although, this is really hard to tell.

As mentioned before Pr is produced through both production processes almost equally, when Ba is produced in larger quantities the $[\text{Pr}/\text{Ba}]$ ratio should decrease somewhat. A very modest decrease with metallicity is seen for $[\text{Pr}/\text{Ba}]$. The $[\text{Mo}/\text{Eu}]$ ratio should increase with metallicity as Mo is produced of a higher rate than Eu when the s -process starts to dominate. This should also be the case for $[\text{Pr}/\text{Eu}]$ but it should increase even faster. In our case a flat trend is presented for subsolar metallicities and at higher metallicity the stars become more scattered, the reason for this high scatter is yet to be explained. Arlandini et al. (1999) also looked at the $[\text{Pr}/\text{Eu}]$ abundance and found that the ratio was flat for subsolar metallicity and at Solar values the ratio increased a bit.

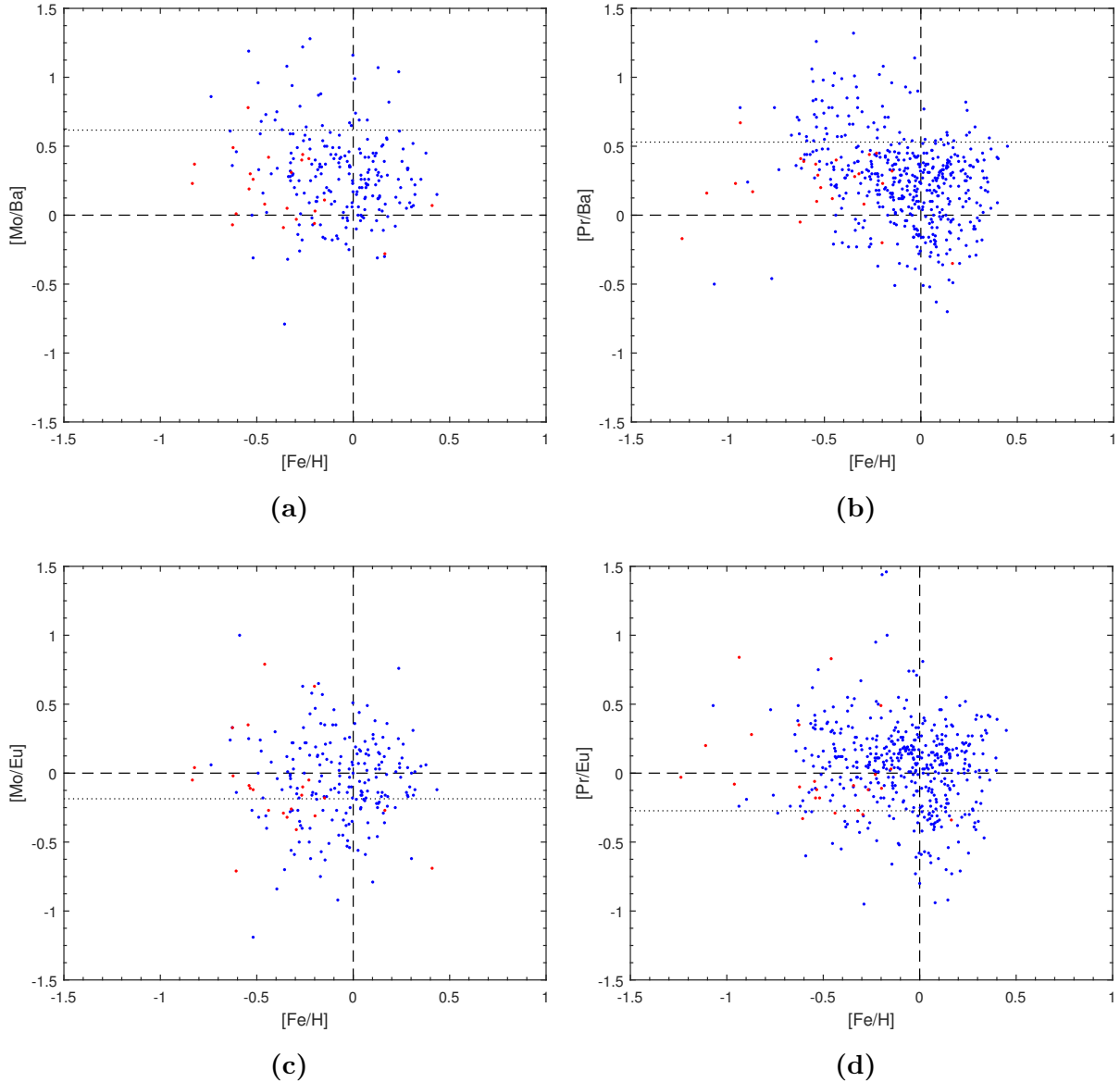


Figure 3.6: $[Mo/Ba]$ and $[Pr/Ba]$ (left and right upper panel, respectively) and $[Mo/Eu]$ and $[Pr/Eu]$ (left and right bottom panel, respectively) as a function of the metallicity $[Fe/H]$. The dotted line represents the pure r-process ratio.

3.2.5 Nd, Sm

The $[Sm/Ba, Eu]$ ratios do not present any trend, as Figure 3.7b and d show. We do observe that the sample is really scattered which suggests that Sm is not that well measured. As for $[Nd/Ba]$, Figure 3.7a, a really modest trend might be seen, that for a decrease in metallicity the $[Nd/Ba]$ ratio increases. The stars are quite scattered though. For Figure 3.7c a mostly flat trend is presented, but for subsolar metallicity the $[Nd/Eu]$ ratio decreases slightly. All

abundance ratios in this figure show that some stars lie at the pure r-process line. This means that Eu and Sm are associated and higher than current models predicts. Compared to the work by Battistini & Bensby (2016) this differs quite a lot, especially for Sm, as they showed an increase in $[Sm/Ba]$ as $[Fe/H]$ decreased. For $[Sm/Eu]$ they showed that the ratio did not increase until Solar metallicity. This might indicate that Sm was not measured that well by GES. For $[Nd/Eu]$ an increase with metallicity was observed. They illustrated a decreasing trend for lower metallicity values for $[Nd/Eu]$.

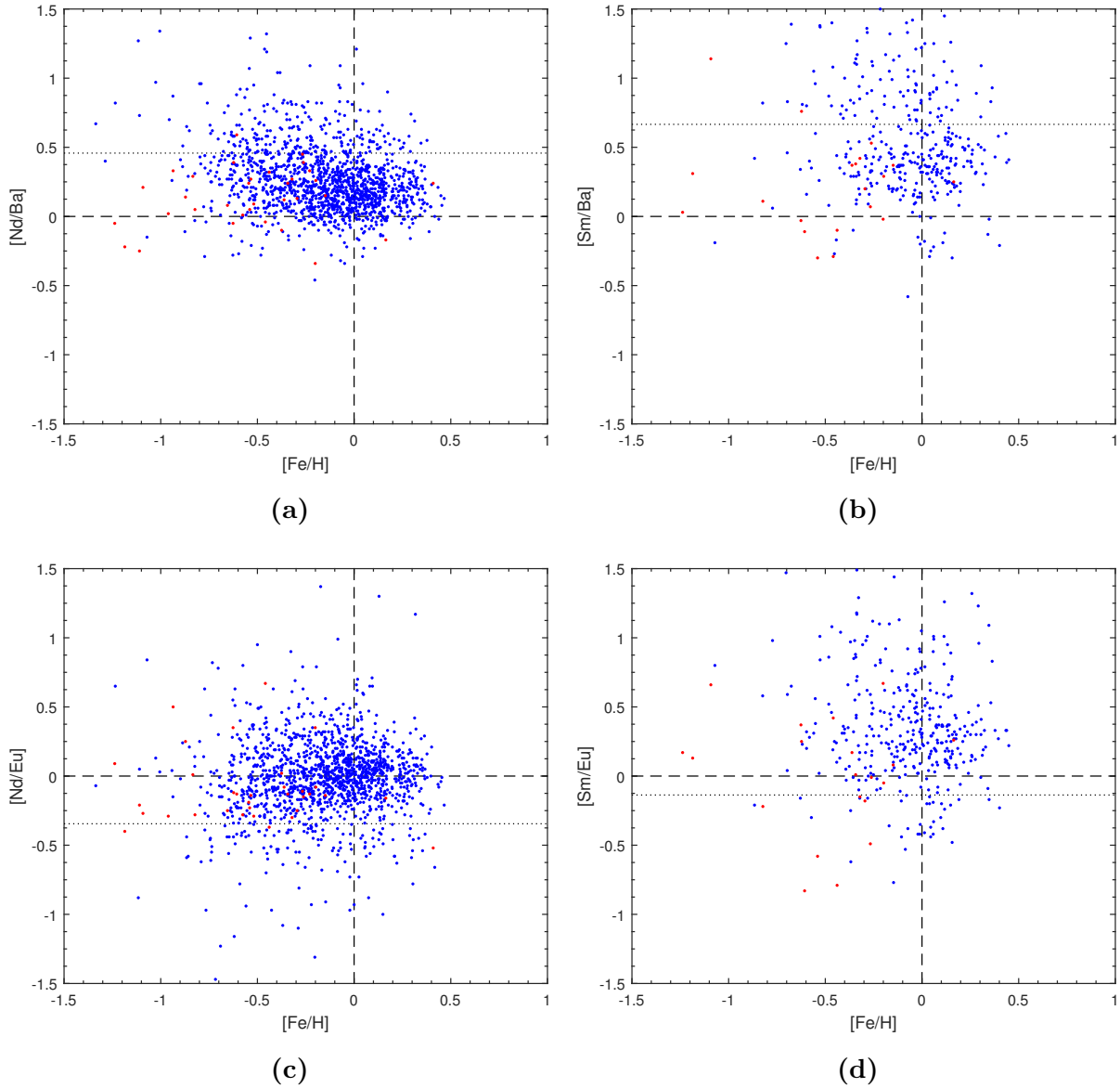
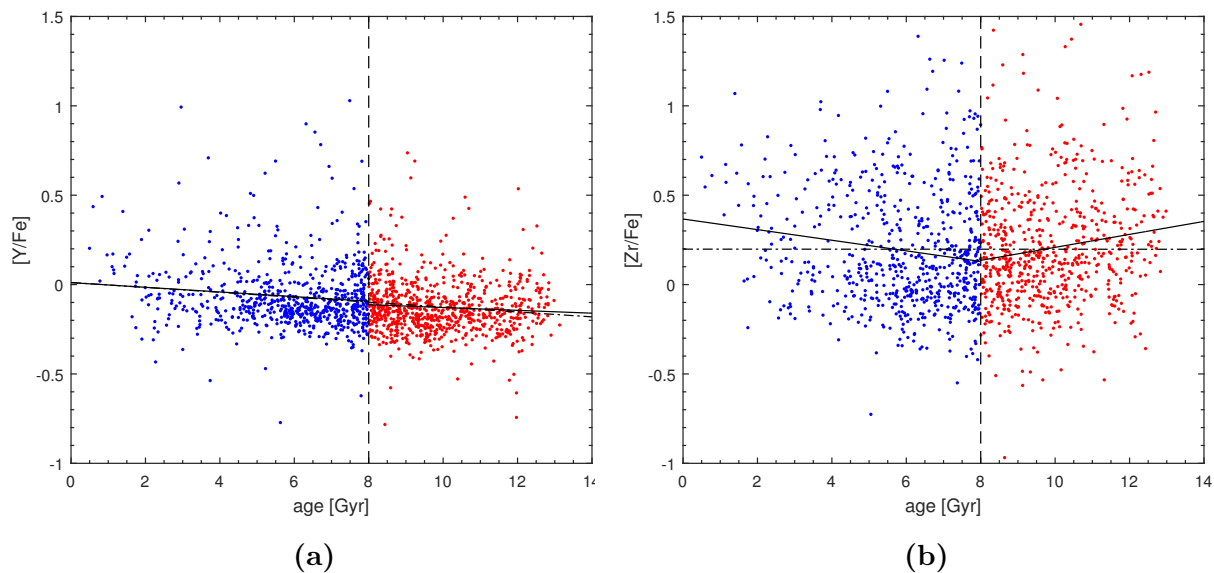
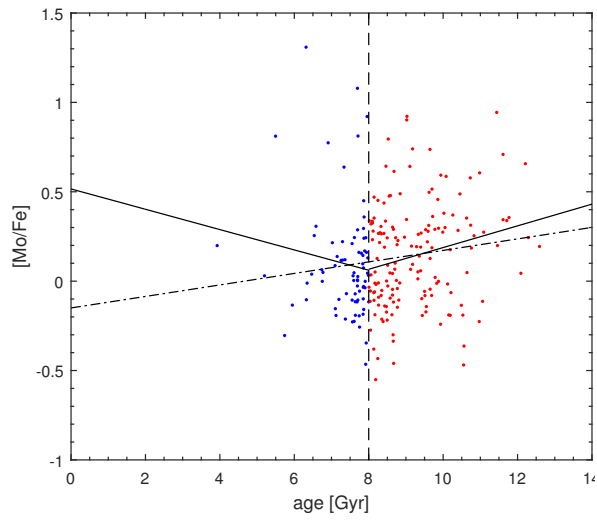


Figure 3.7: $[Nd/Ba]$ and $[Sm/Ba]$ (left and right upper panel, respectively) and $[Nd/Eu]$ and $[Sm/Eu]$ (left and right bottom panel, respectively) as a function of the metallicity $[Fe/H]$. The dotted line represents the pure r-process ratio.

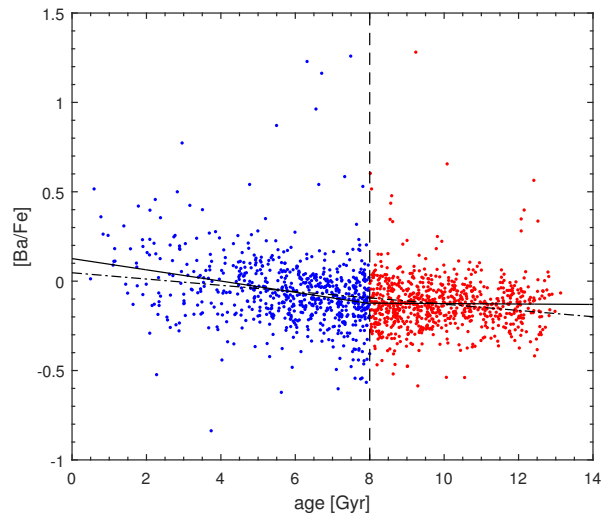
3.3 Abundances ratio compared to age

To distinguish between thin and thick disc stars, the same limit used by Battistini & Bensby (2016), i.e. that stars older than 8 Gyr belong to the thick disc and stars younger than that can be found in the thin disc is used here. Note that there are other methods to distinguish the discs from each other, for example by the stars kinematics or their α -abundance for a given metallicity. The abundance ratio, $[x/Fe]$ was plotted as a function of the ages, which were calculated using the methods of Serenelli et al. (2013), to see how they varied with time. The average error of the age is about 3 Gyr. Figure 3.8 shows the outcome of this. A black linear line to indicate the best fit for the thin and thick disc stars was introduced in the figures together with a linear fit for the whole data set (dashed line).

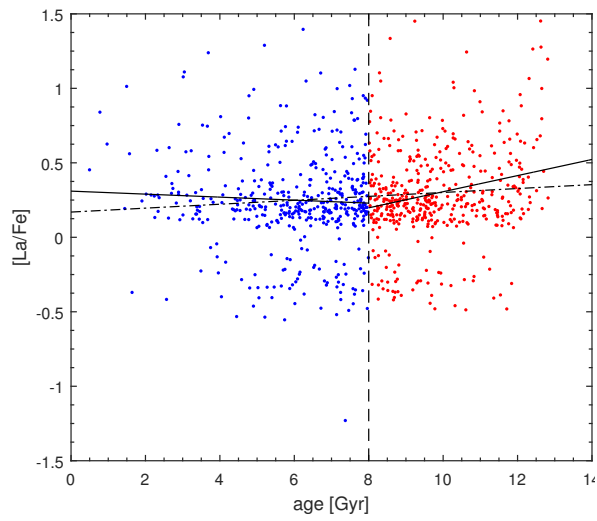




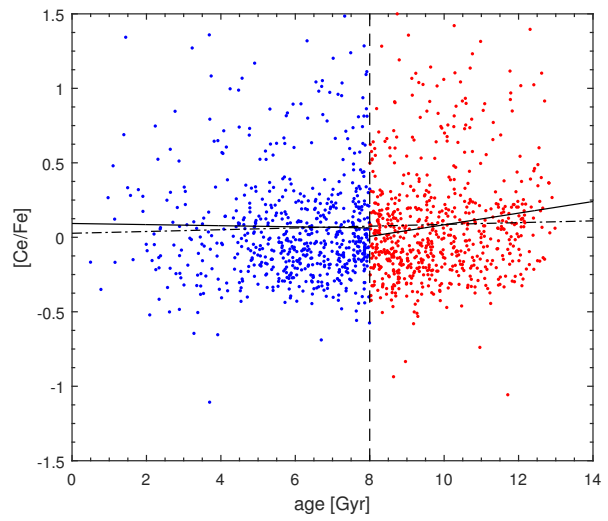
(c)



(d)



(e)



(f)

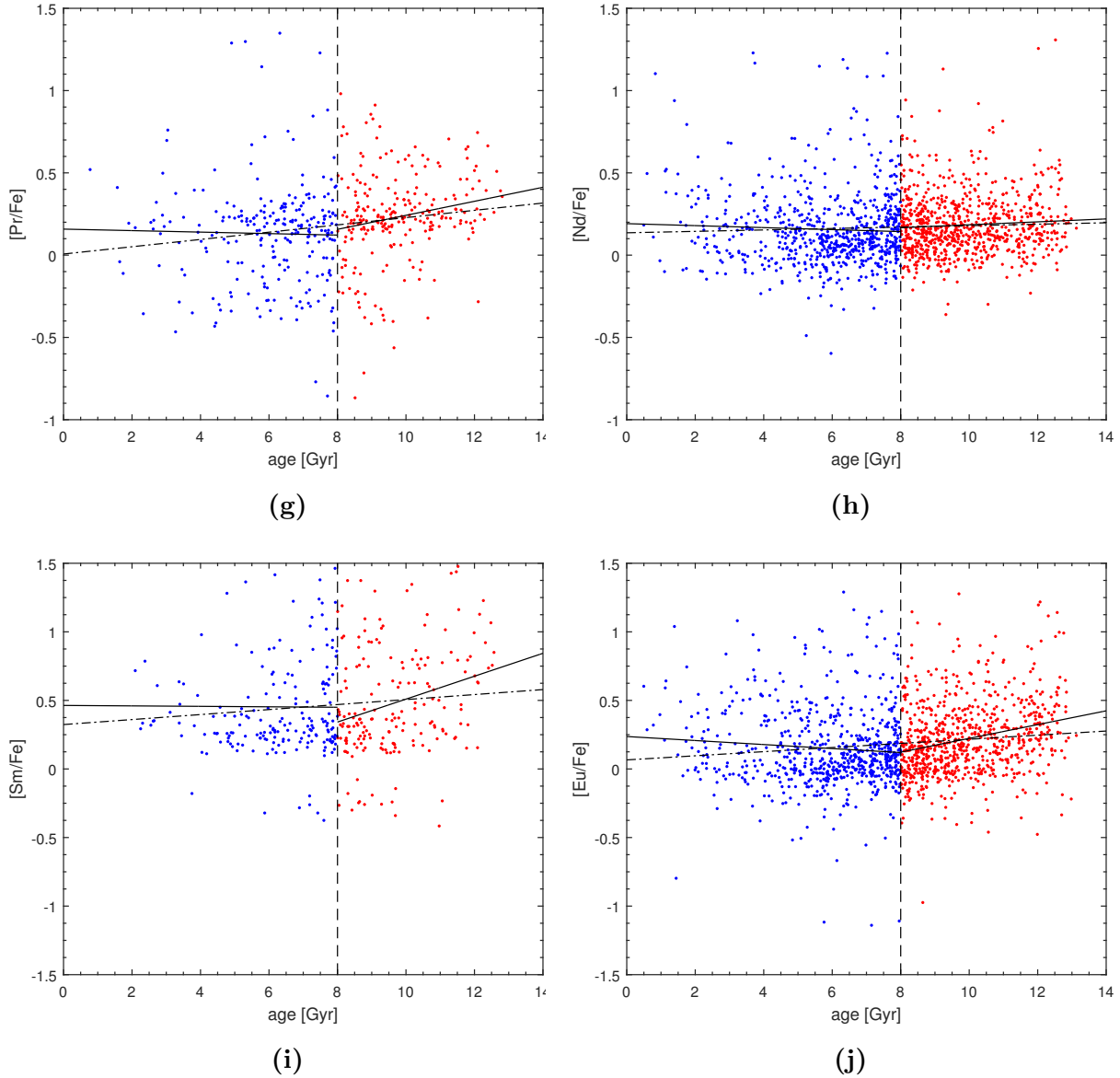


Figure 3.8: *The abundance ratio, $[x/Fe]$, as a function of age. Here the red dots represent stars older than 8 Gyr and blue dots are stars younger than 8 Gyr. The black lines demonstrate the best fit for the thin and thick disc, respectively. The black dotted line shows the best fit for all stars.*

A change in slope can be seen for most of the elements in Figure 3.8. Only for Y and Nd, in Fig. 3.8a and h, is the slope almost flat through the whole data set. For the rest of the elements the slope changes around 8 Gyr. For Y the flat trend in the thin disc is expected as there are more stars that have higher Y abundance. The flatness in the thick disc is unexpected though.

For Zr and Mo in Figure 3.8b and c, the linear fit decreases with $[Zr,Mo/Fe]$ as the

age of the thin disc stars increases. This can be due to the fact that Zr is created mainly through the *s*-process, which is the leading process when it comes to enrich the thin disc. For Mo this is not the case as it is produced mostly through the *r*-process. One explanation could be the fact that the stars are too scattered and few in the thin disc to make a good linear fit, which implies that Mo is harder to measure in younger stars. After 8 Gyr, the thick disc stars get an increase in their abundance ratio as they get older. For [Zr/Fe] this is remarkable, as it should be quite low for an element that is mainly produced via the *s*-process. Battistini & Bensby (2016) showed that this was the case for [Zr/Fe] as well, and suggests this could be because of LEPP.

Figure 3.8d shows a slight increase in [Ba/Fe] as the thin disc stars ages decreased. After 8 Gyr, the slope flattens out for the thick disc stars. This indicates that the enrichment by the *s*-process in the thin disc has increased the Ba abundance ratio, which should be the case as it is produced through this process almost only. The flat trend for thick disc stars also confirms this.

For La, Ce, Pr, Sm and Eu (Fig. 3.8e, f, g, i and j) the trend for the thin disc stars is quite flat. This implies that the AGB stars with low- and intermediate mass have become more influential which would explain the flatness of the young stars, since the Fe production from SN Ia is similar to this. The neutron-capture elements will increase as the metallicity increases as well. This could also explain the flatness for the thin disc stars in Nd. As for the stars older than 8 Gyr, the abundance ratio increases with ageing. This means that in the early evolution of the Milky Way the neutron-capture enrichment was higher, even though it was only by the *r*-process from the massive stars. This could describe the decreasing Mo abundance ratio with decreasing age, for the thick disc stars too.

The flat trend illustrated by most of the thin disc stars (Y, La, Ce, Pr, Nd, Sm and Eu) matches the result by Battistini & Bensby (2016) as well. The abundance ratio for La, Ce, Nd, Sm and Eu were flat in their case too. The increasing trend for Mo, La, Ce, Pr, Sm and Eu for the thick disc stars was also shown by Battistini & Bensby (2016). They on the other hand got a flat trend for stars older than 8 Gyr for [Ce/Fe]. The [Nd/Fe] ratio as a function of age was not that flat for the thick disc stars as it is in our case. But overall the result is somewhat similar.

3.4 Position of the stars

The *z*-position is defined as the height above the Galactic plane. The absolute *z*-position of each star was plotted as a function of age, see Figure 3.9, both ages and distances to the stars are calculated using the methods of Serenelli et al. (2013). From this picture it is clearly seen that the stars get more spread out from the Galactic plane with age. The colour of the star illustrates the metallicity, and here metallicity decreases with age, as expected. Figure 3.10 presents the absolute *z*-position as a function of the abundance ratio for the investigated elements, as before, the colour represents the metallicity. The black line is the best linear fit to the data set.

Figure 3.10a and d show the expected result for the *s*-process element Y and Ba.

However, Zr and La are also typical s -process element and should show similarities to Y and Ba. The fact that they seem to increase in metallicity as the z -position increase is interesting (see Fig. 3.10b and e). This suggest that Zr and La are more abundant in older stars, which implies that they were created trough another process at a higher rate in the young Galaxy compared to Fe. Another explanation could be the gap in La (see Section 3.1.7), and the large scatter for higher metallicity which make the best fit hard to determine. LEPP could be the explanation to why Zr differ.

The r -process elements in Fig. 3.10c, i and j all have the expected gradient, as they should be more abundant in low metallicity stars.

Because Pr and Nd are both created almost equally through both processes they should show similarities to each other. Both do increase in abundance ratio for larger z -position but Pr increases much faster, suggesting it is created mainly by the r -process. Since Pr has fewer stars, this might explain the differences. It can also be that it is produced via the r -process in a higher extent.

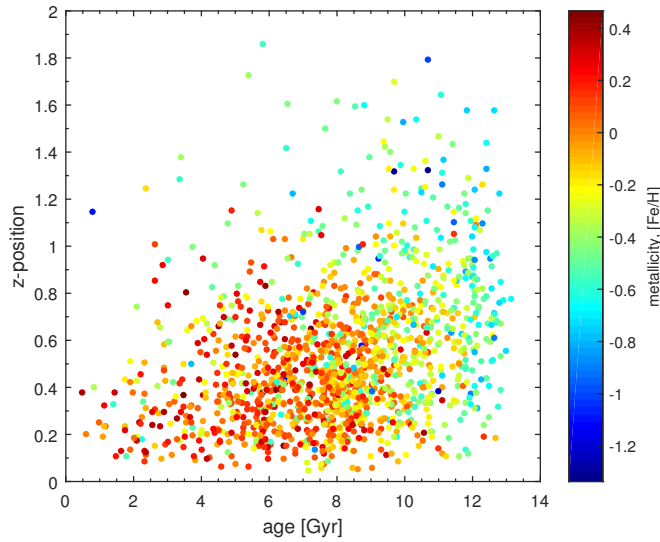
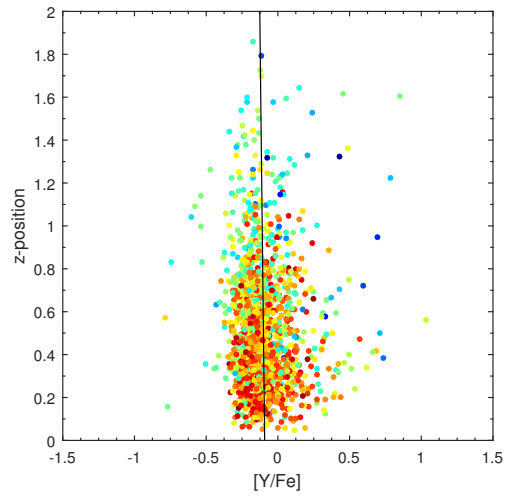
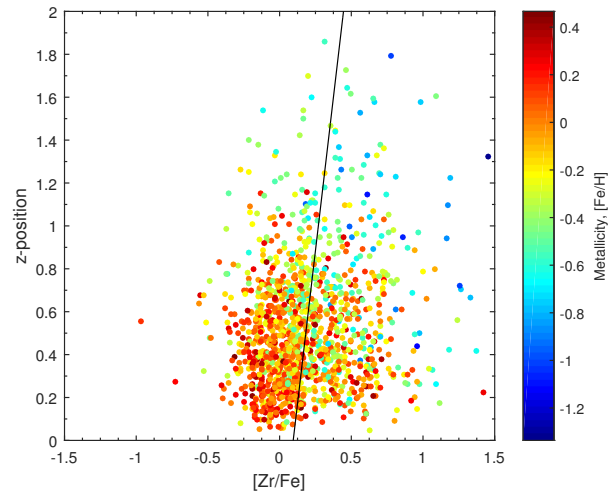


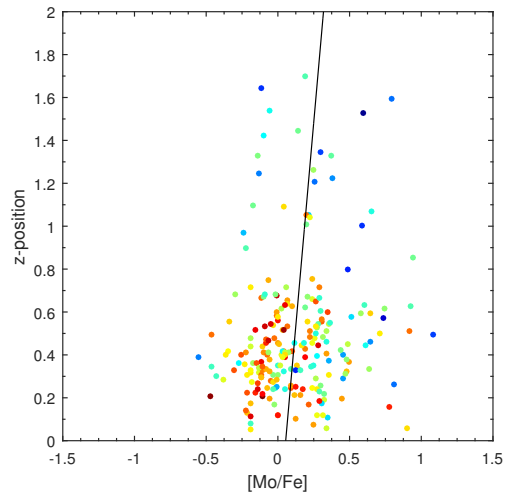
Figure 3.9: *The absolute z -position, $|z| = 0$ at Galactic center, plotted against the stars ages. The metallicity is represented by a colour.*



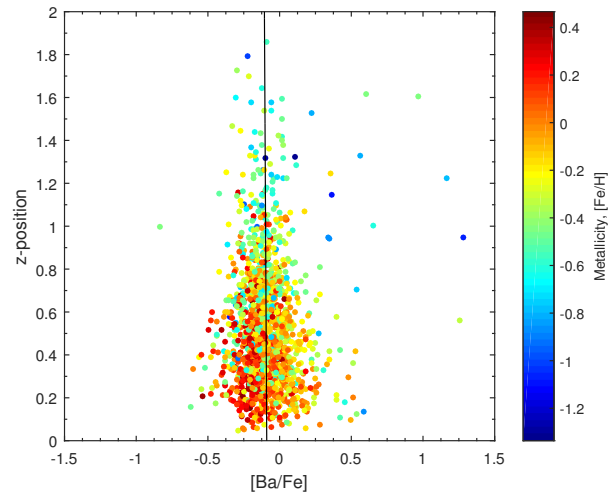
(a)



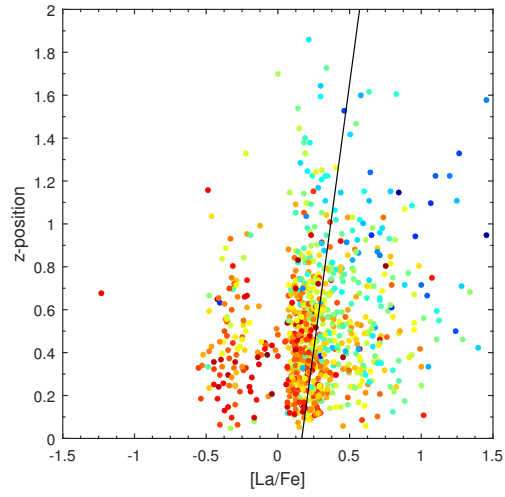
(b)



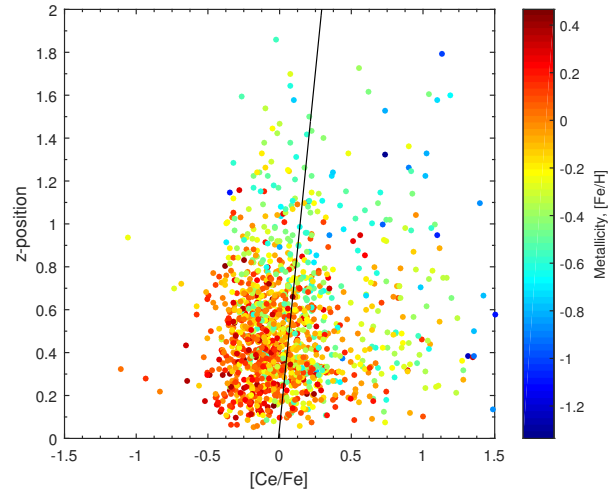
(c)



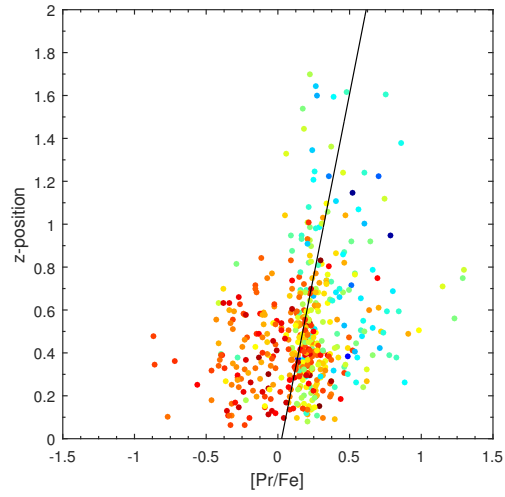
(d)



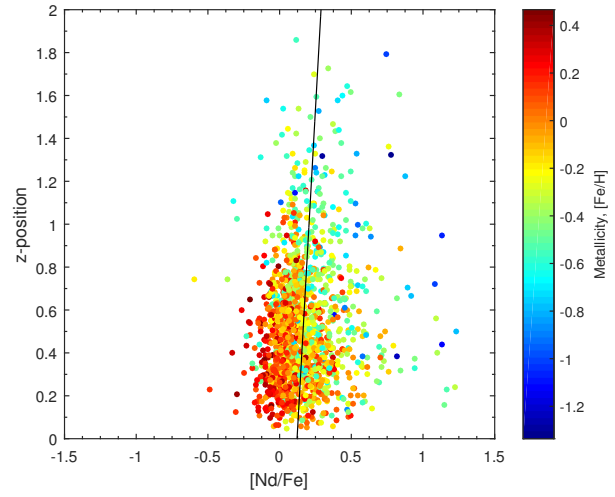
(e)



(f)



(g)



(h)

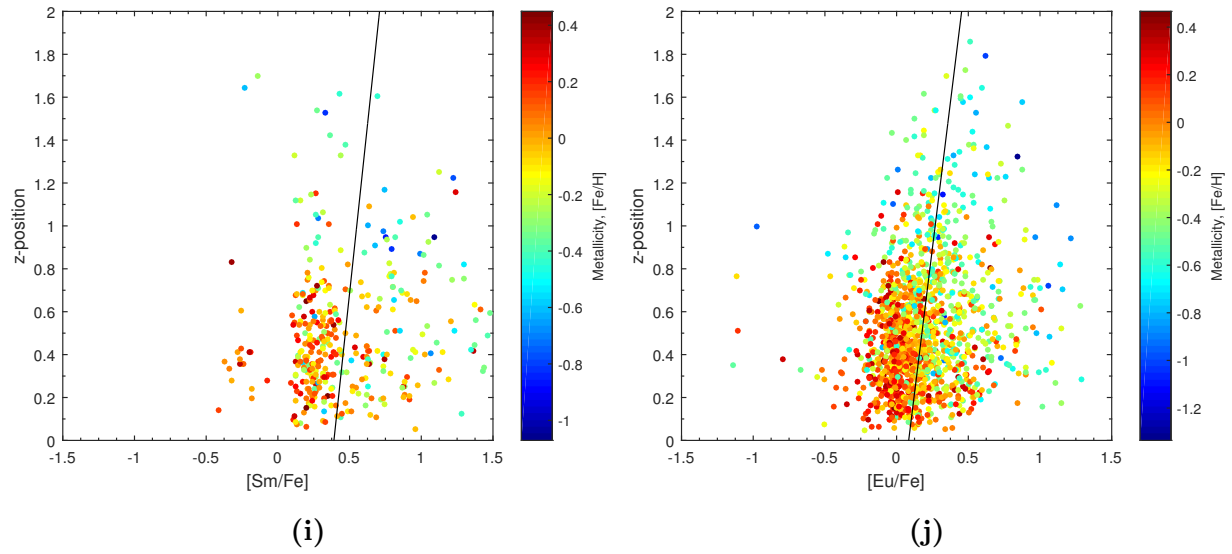


Figure 3.10: *The absolute z -position as a function of the abundance ratio, $[x/Fe]$. The stars metallicity is represented by a colour. The black line illustrates the best linear fit to the data.*

Chapter 4

Conclusions

To study the formation and evolution of the thin and thick disc, 10 different neutron-capture elements were analysed. An abundance analysis was done for the field stars measured by Gaia-ESO, which has released measurements for neutron-capture elements in many more stars than ever studied before. The data for the neutron-capture elements from GES has not been investigated before either. The data was double checked and confirmed by matching it with known literature and by checking the spectral lines and abundance ratio in SME, which gave promising results. In total 1486 stars were investigated. After making the limitations stated in the introduction and concluding that stars with S/N lower than 12 should be taken out of the sample, the initial results could be produced and discussed.

The abundance ratio as a function of metallicity (Fig. 3.2) shows promising results, although, the gap in La, Pr and Sm cannot be explained, an indication that the data is not perfect. The gaps makes it hard to see any relation between the stars and also to compare with earlier work, this might be an explanation to why La and Sm differs so much compared to Battistini & Bensby (2016). Some similarities with previous work by Battistini & Bensby (2016) and Bensby et al. (2014) were found, even though our data included many more stars, with larger errors.

The overall trend was increasing abundance ratio with decreasing metallicity, which indicates that many of the neutron-capture elements were present in the early evolution of the Milky Way. Even though we think the *r*-process was the only active neutron-capture process at that time many elements were created through this process, but as the Galaxy got older and bigger the *s*-process started kicking in as the AGB stars developed. This mean that some *r*-process elements, such as Mo, Sm and Eu should decrease with metallicity. This is indeed the case for Eu, but for Mo and Sm this trend is not as clear since the stars are so scattered and few. The trends for La and Ce are not that obvious, but a slight increase in their abundance ratio is seen for lower metallicity. Pr and Nd show that the abundance ratio decreases for higher metallicity, as they are created through both processes more or less equally. This means that the *r*-process in the early Galaxy contained higher abundance ratios compared to the metallicity. Because Y and Zr come from the same *s*-process peak, they should show similar results. This is not seen at all. Y shows a

flat trend and Zr a decreasing trend with $[\text{Fe}/\text{H}]$. The same trend is observed in Bensby et al. (2014) and Battistini & Bensby (2016), respectively, this unexpected difference could be due to LEPP. This work confirms another s -process production channel is needed to explain the differences in our Y and Zr results.

When looking at the origin of the r - and s -process plots, they differed compared to earlier results done by Battistini & Bensby (2016). The same trend is seen in most of the elements although much fainter. This could be explained by the fact that we measured so many more stars and that they are more scattered and have a larger error. For Sm the differences is so large it suggests that it is not well measured.

The abundance ratio plotted against age compared to Battistini & Bensby (2016) were similar, which helps confirm the validity of our results. A change in slope is seen for nearly all elements around 8 Gyr, which coincides with the proposed age limit between the thin and thick disc. The majority of the elements show a flat tendency for the young thin disc stars. This flatness can be due to the fact that the s -process production is in balance with the Fe production from type-Ia supernovae. An increase in abundance ratio for the older thick disc stars was illustrated for most of the elements meaning that the production of neutron-capture elements was higher in the young Milky Way. As the stars get younger and the Galaxy older this tendency decreases most likely because the SN II decreases with time too, which results in a lower enrichment for elements created through the r -process.

By studying the z -position as a function of age it was seen from Figure 3.9 that the older a star got, the further out from the Galactic plane it was, as expected. It shows that older stars are metal-poor and younger stars are metal-rich, as expected. When plotting the z -position as a function of abundance ratio (Fig. 3.10) the general trend showed an increasing abundance ratio for higher z -position values. Which is expected from r -process elements like Mo, Sm and Eu. For elements like Zr, Pr and La this is quite surprising. Zr and La are s -process elements and should show similarities to Y and Ba, which showed a flat trend. This suggest that Zr and La are more abundant in older star, which implies that they were created through the r -process at a higher rate in the early formation of the Milky Way. Pr on the other hand should show a similar trend to Nd, our result showed a Pr-trend that grows much faster, indicating that it is produced via the r -process in a higher extent.

4.1 Future work

- Since some stars showed high $[\text{x}/\text{Fe}]$ abundance ratio, in future work, a good idea would be to check why this is. This could be done by re-measuring the lines, individually checking the spectra or getting new observations for example.
- The temperature dependence in $[\text{Ba}/\text{Fe}]$ would also need to be investigated, it cannot only be due to the fact that Ba suffers from NLTE at $T_{eff} > 6100$ K, since the dependence seems to start around $T_{eff} \approx 5500$ K in our case.

- Gaia-ESO also measured the distance of the stars, this information can be used to check how many of the stars lie further out from the Galactic plane and how far from the Galactic center they are.
- One improvement would be to calculate an average error and present it in the corner of the abundance ratio against the metallicity figures, which would be helpful for the reader.
- Another improvement might be to make contour plots for the $[x/Fe]$ - $[Fe/H]$ abundance plane. In that way, one could better see where there are large amount of stars and the trends would probably become even more clear.
- Another idea would be to distinguish between thin and thick disc stars in the $[x/Ba, Eu]$ (as mention in section 3.2 it is good to compare our elements with Ba and Eu, as these two elements is mostly produce through the s -process and the r -process, respectively) plots as a function of metallicity, as Battistini & Bensby (2016) do. In that way it can be checked if indeed the thick disc stars are closer to the derived r -process line as they should be.
- To explain the results presented for Mo and Pr which rarely is observed, a project where one focuses on these two neutron-capture elements would be good. The fact that Mo seems to be hard to measure in young stars is worth investigating and trying to get more and better observations for this element.
- One should also try to remeasure Sm as the high scatter in the $[Sm/Ba, Eu]$ against $[Fe/H]$ implies that this element was not that well measured.
- Improvements to the nucleosynthetic models are also needed, as the difference seen in Y and Zr implies that some new s -process production (e.g. LEPP) is needed to explain this difference.
- The high $[Eu/Ba]$ stars also suggest that the r -process models do not produce enough Eu, which indicates that the nucleosynthetic models needs to be improved.

Bibliography

- Arlandini, C., Käppeler, F., Wisshak, K., et al. 1999, ApJ, 525, 886
- Asplund, M., Grevesse, N., Sauval, A. J., & Scott, P. 2009, ARA&A, 47, 481
- Battistini, C. & Bensby, T. 2016, A&A, 586, A49
- Bensby, T., Feltzing, S., & Oey, M. S. 2014, A&A, 562, A71
- Bisterzo, S., Travaglio, C., Gallino, R., Wiescher, M., & Käppeler, F. 2014, ApJ, 787, 10
- Burbidge, E. M., Burbidge, G. R., Fowler, W. A., & Hoyle, F. 1957, Reviews of Modern Physics, 29, 547
- Burris, D. L., Pilachowski, C. A., Armandroff, T. E., et al. 2000, ApJ, 544, 302
- Carretta, E., Lucatello, S., Gratton, R. G., Bragaglia, A., & D’Orazi, V. 2011, A&A, 533, A69
- Cescutti, G., Chiappini, C., Hirschi, R., Meynet, G., & Frischknecht, U. 2013, A&A, 553, A51
- Dekker, H., D’Odorico, S., Kaufer, A., Delabre, B., & Kotzlowski, H. 2000, in Optical and IR Telescope Instrumentation and Detectors, ed. M. Iye & A. F. Moorwood, Vol. 4008, 534–545
- Fishlock, C. K., Karakas, A. I., Lugaro, M., & Yong, D. 2014, ApJ, 797, 44
- Freiburghaus, C., Rosswog, S., & Thielemann, F.-K. 1999, ApJ, 525, L121
- Fulbright, J. P. 2000, AJ, 120, 1841
- Gilmore, G., Randich, S., Asplund, M., et al. 2012, The Messenger, 147, 25
- Gustafsson, B., Edvardsson, B., Eriksson, K., et al. 2008, A&A, 486, 951
- Heiter, U., Jofré, P., Gustafsson, B., et al. 2015, A&A, 582, A49
- Karakas, A. I. & Lugaro, M. 2016, ApJ, 825, 26

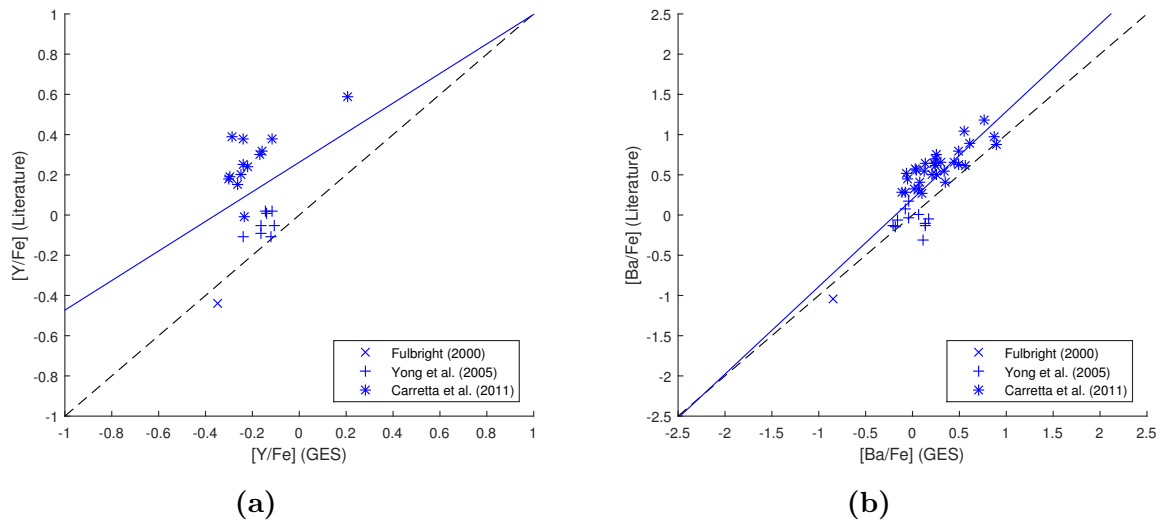
- Koch, A. & Edvardsson, B. 2002, *A&A*, 381, 500
- Korotin, S., Mishenina, T., Gorbaneva, T., & Soubiran, C. 2011, *MNRAS*, 415, 2093
- Mashonkina, L. I., Vinogradova, A. B., Ptitsyn, D. A., Khokhlova, V. S., & Chernetsova, T. A. 2007, *Astron. Rep.*, 51, 903
- Mishenina, T. V., Pignatari, M., Korotin, S. A., et al. 2013, *A&A*, 552, A128
- Pancino, E., Lardo, C., Altavilla, G., et al. 2017, *A&A*, 598, A5
- Prialink, D. 2010, *An introduction to the Theory of Stella Structure and Evolution* (Cambridge University Press)
- Reddy, B. E., Lambert, D. L., & Allende Prieto, C. 2006, *MNRAS*, 367, 1329
- Serenelli, A. M., Bergemann, M., Ruchti, G., & Casagrande, L. 2013, *MNRAS*, 429, 3645
- Snedden, C., Cowan, J. J., & Gallino, R. 2008, *ARA&A*, 46, 241
- Stonkutė, E., Kozlov, S. E., Howes, L. M., et al. 2016, *MNRAS*, 460, 1131
- Travaglio, C., Gallino, R., Arnone, E., et al. 2004, *ApJ*, 601, 864
- Valenti, J. A. & Fischer, D. A. 2005, *ApJS*, 159, 141
- Valenti, J. A. & Piskunov, N. 1996, *A&AS*, 118, 595
- Yong, D., Grundahl, F., Nissen, P. E., Jensen, H. R., & Lambert, D. L. 2005, *A&A*, 438, 875

Appendices

Appendix A

GES match with literature

Here the rest of the figures from the match between GES and Fulbright (2000), Koch & Edvardsson (2002), Yong et al. (2005), Carretta et al. (2011) and Battistini & Bensby (2016) are presented in Figure A.1. Figure A.2 illustrates the remaining images for the abundance difference between GES and the literature as a function of S/N and abundance error.



APPENDIX A. GES MATCH WITH LITERATURE

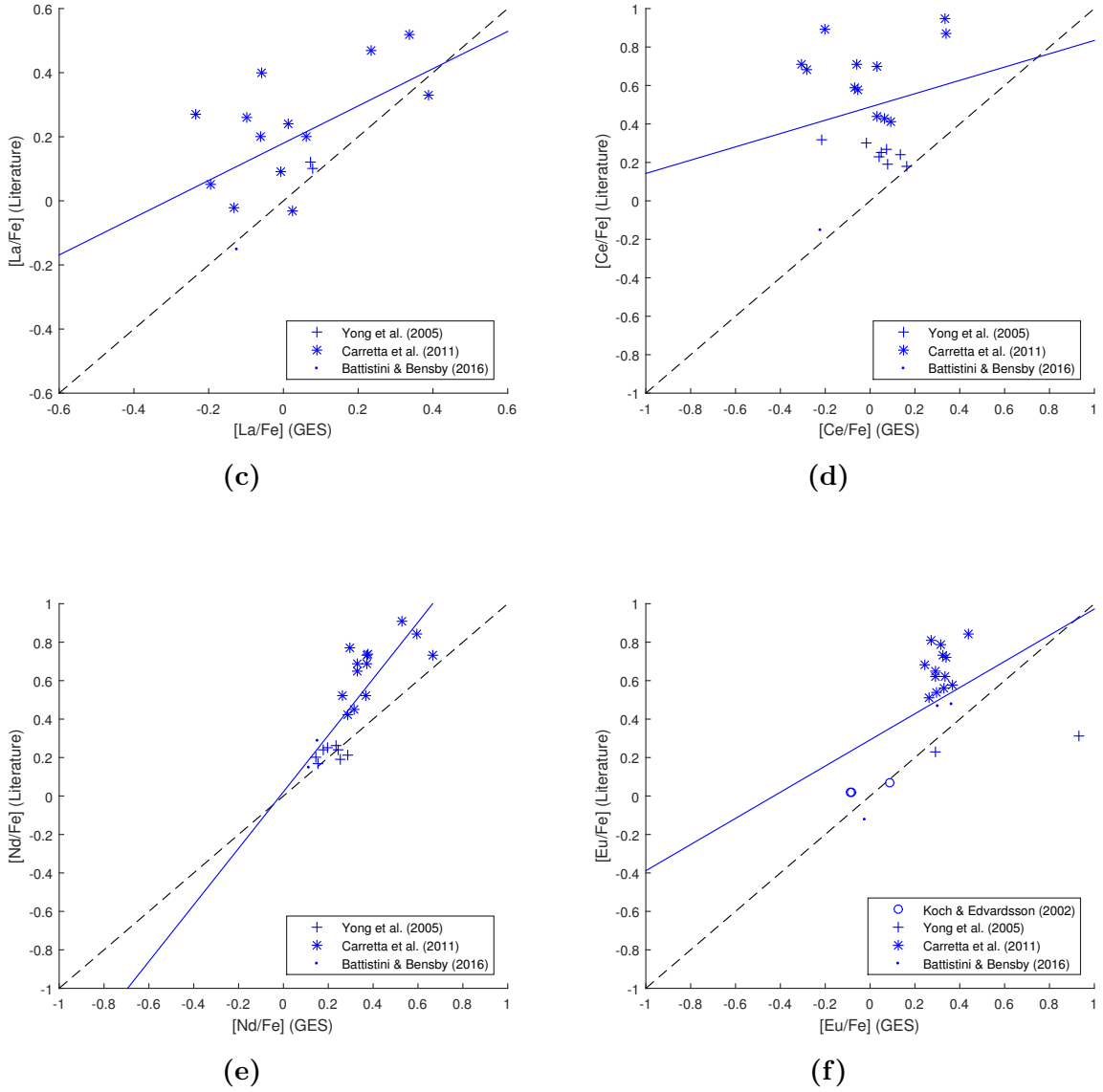
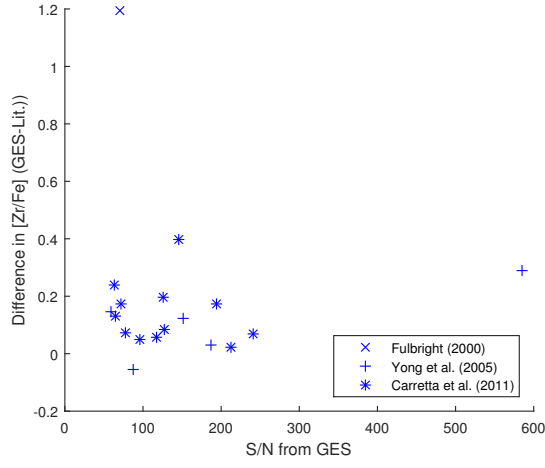
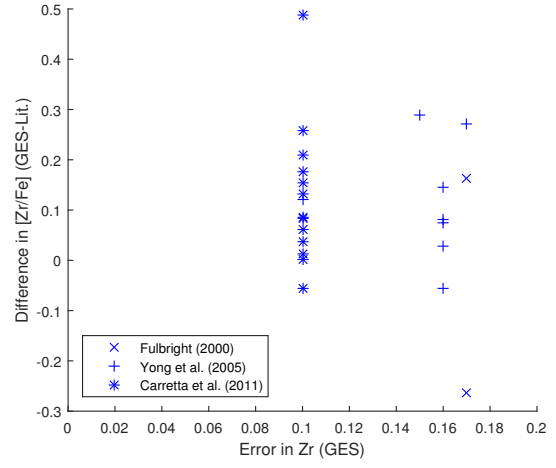


Figure A.1: The literature abundance ratio, $[x/Fe]$ against the GES abundance ratio. The blue line shows the best linear fit to the data. The black dashed line is the 1 : 1 ratio.

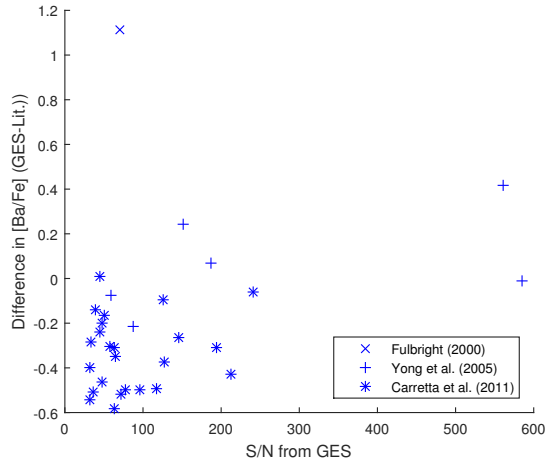
APPENDIX A. GES MATCH WITH LITERATURE



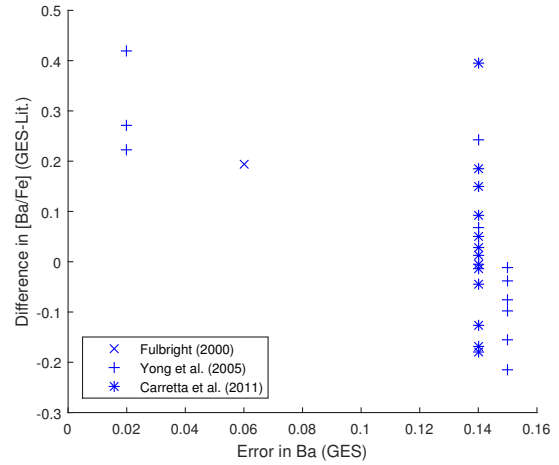
(a)



(b)

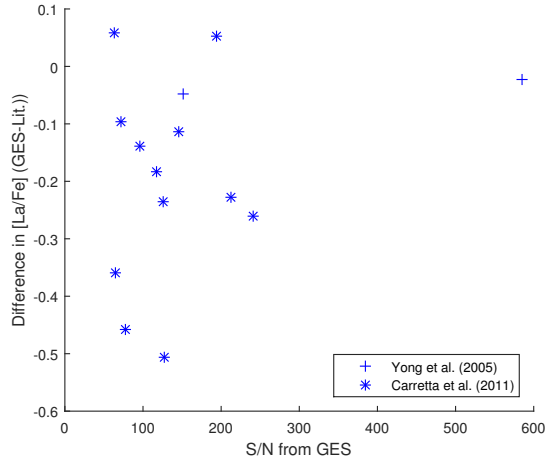


(c)

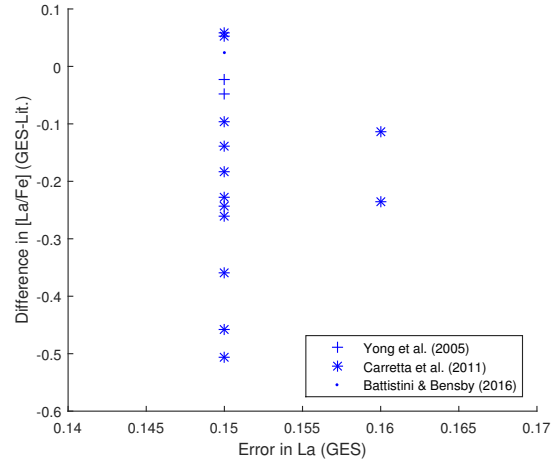


(d)

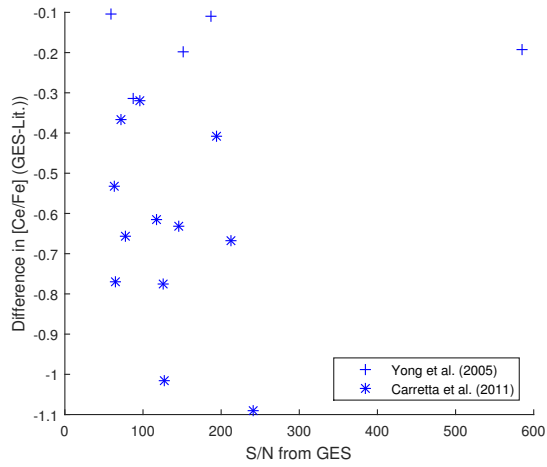
APPENDIX A. GES MATCH WITH LITERATURE



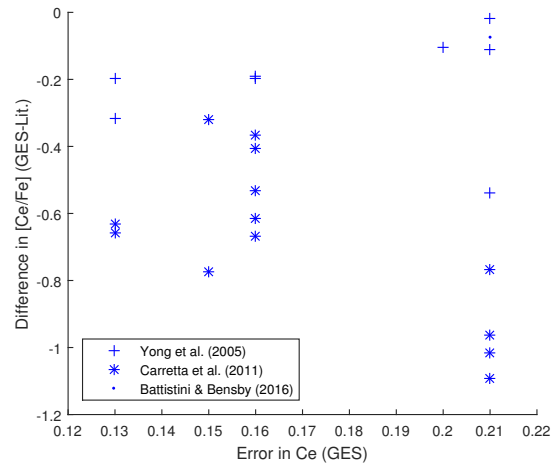
(e)



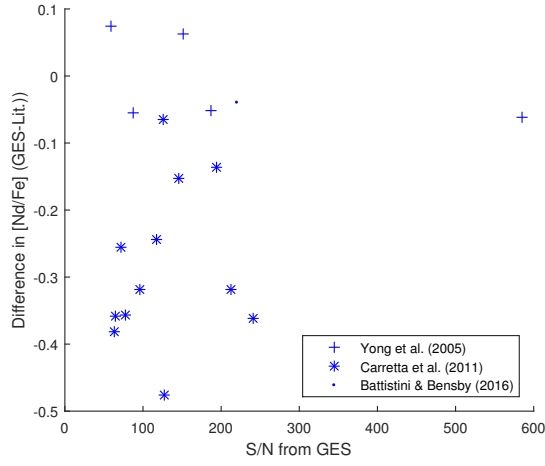
(f)



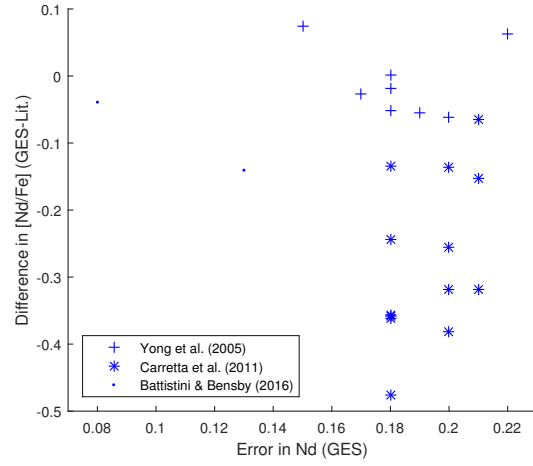
(g)



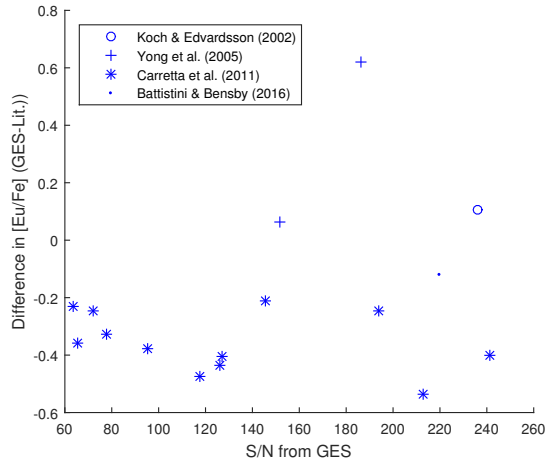
(h)



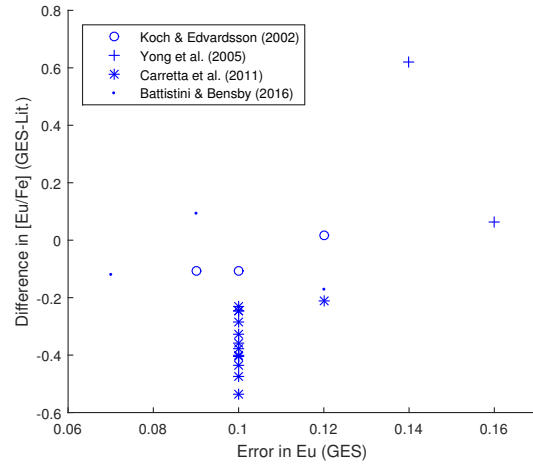
(i)



(j)



(k)



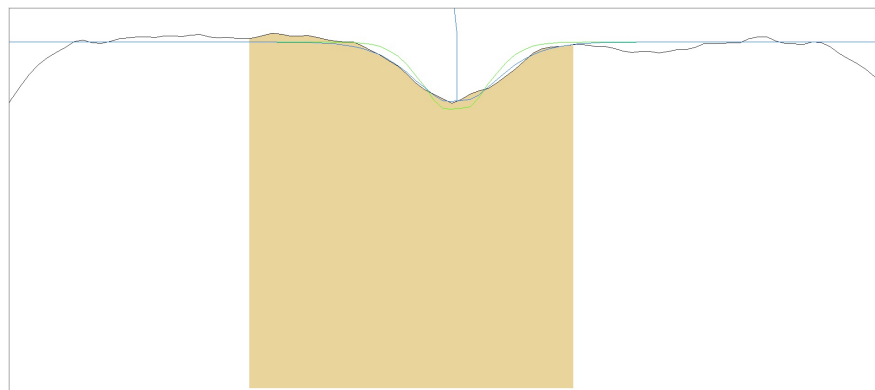
(l)

Figure A.2: The difference in $[x/Fe]$ against the signal-to-noise ratio (left panel) or error in x (right panel).

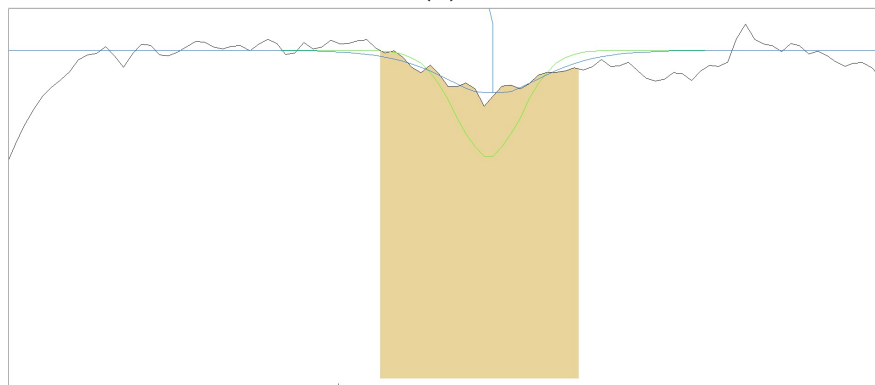
Appendix B

SME example

Here in Figure B.1, an example of how SME fitted the Ce II 5274.229 Å line for our four different stars (from Table 2.3) can be seen. The black line is the observed spectrum, the green line is the initial fit and the blue line is the final fit of the calculated synthetic spectrum. The dark yellow region marks the line. The light yellow region marks the continuum.



(a)



(b)

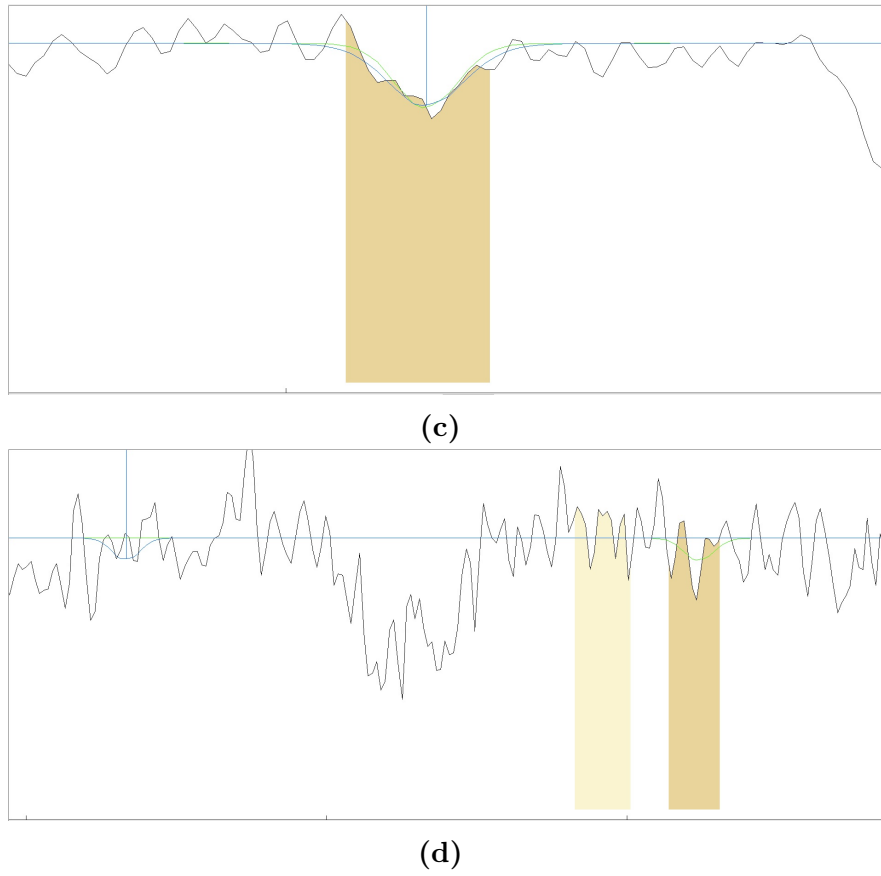
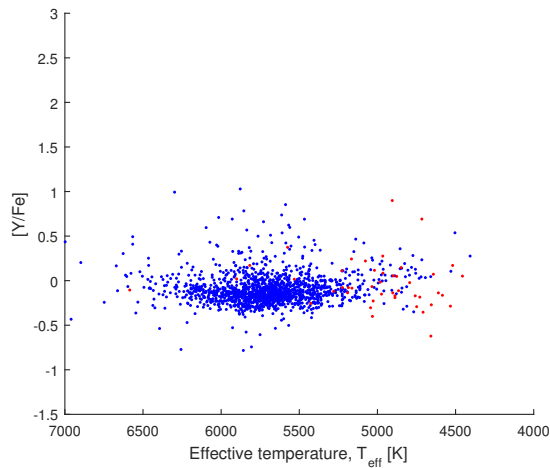


Figure B.1: Here, an example of how the calculated spectrum from SME fitted the observed spectrum for the Ce II 5274.229 Å line for the (a) $S/N \approx 212$ star, (b) $S/N \approx 55$ star, (c) $S/N \approx 15$ star and (d) $S/N \approx 9$ star is seen.

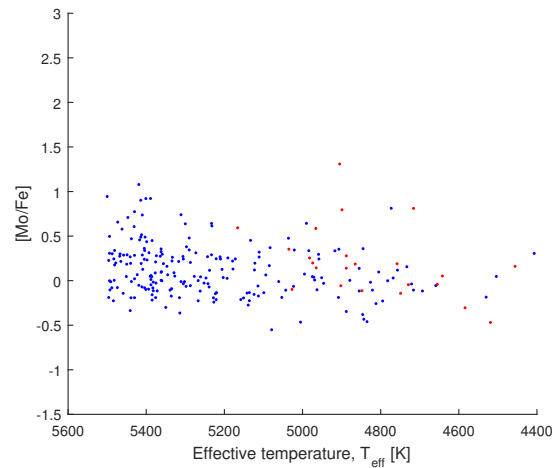
Appendix C

Abundance ratio as a function of temperature

The remaining figures of the abundance ratio as a function of the effective temperature is showed in Figure C.1 below.

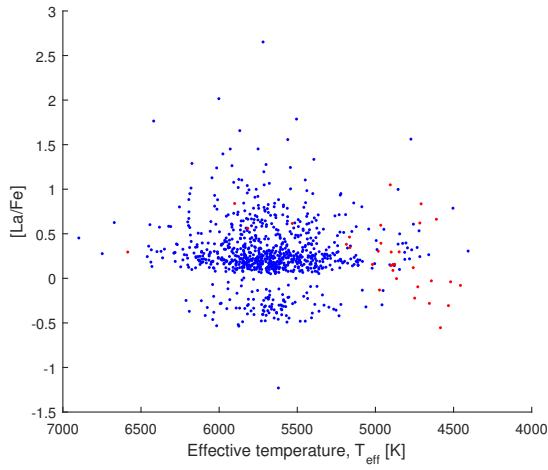


(a)

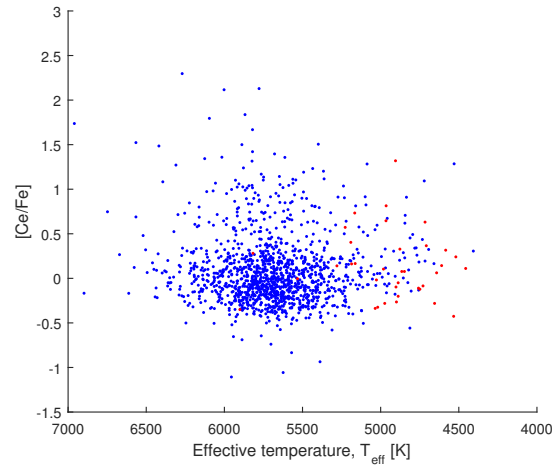


(b)

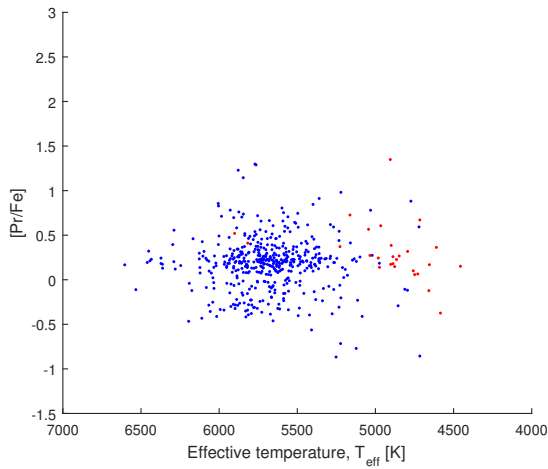
APPENDIX C. ABUNDANCE RATIO AS A FUNCTION OF TEMPERATURE



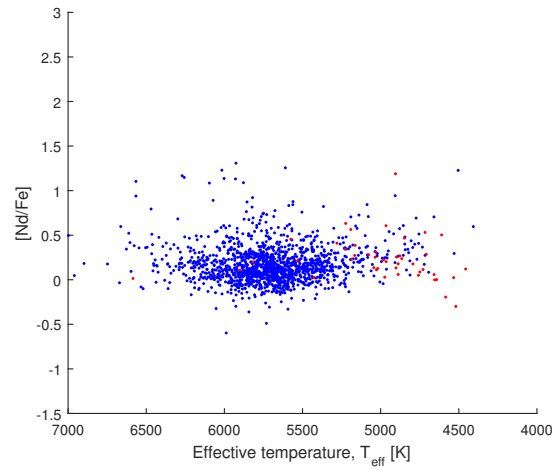
(c)



(d)



(e)



(f)

APPENDIX C. ABUNDANCE RATIO AS A FUNCTION OF TEMPERATURE

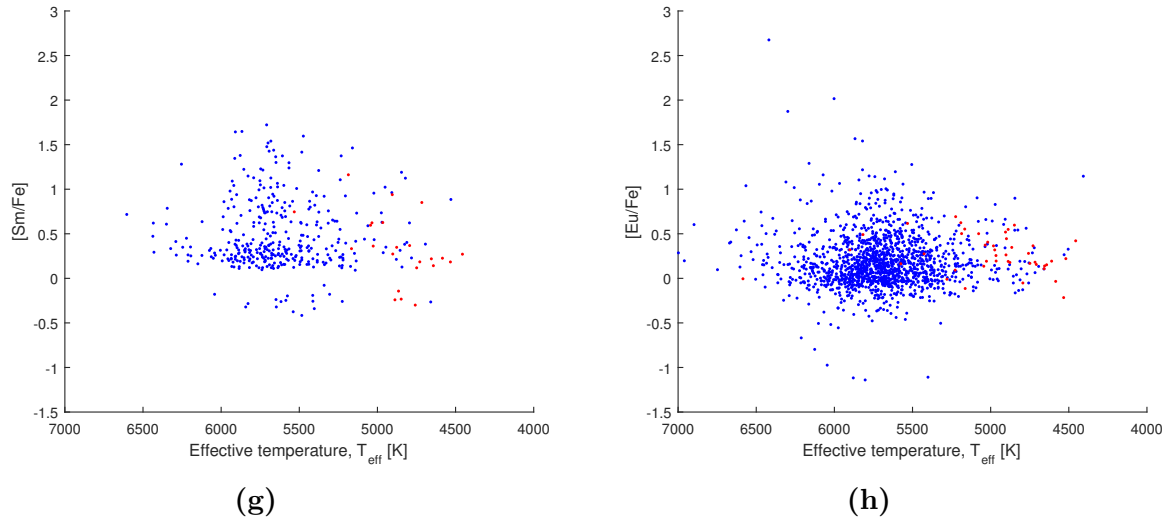


Figure C.1: *The abundance ratio, $[x/Fe]$, as a function of effective temperature, T_{eff} .*